University of Tennessee, Knoxville

TRACE: Tennessee Research and Creative Exchange

Masters Theses

Graduate School

12-2004

A Two-Phase Cooling Method Using R134a Refrigerant to Cool Power Electronics Devices

Jeremy Bryant Campbell
University of Tennessee - Knoxville

Follow this and additional works at: https://trace.tennessee.edu/utk_gradthes

Part of the Electrical and Computer Engineering Commons

Recommended Citation

Campbell, Jeremy Bryant, "A Two-Phase Cooling Method Using R134a Refrigerant to Cool Power Electronics Devices. " Master's Thesis, University of Tennessee, 2004.
https://trace.tennessee.edu/utk_gradthes/1893

This Thesis is brought to you for free and open access by the Graduate School at TRACE: Tennessee Research and Creative Exchange. It has been accepted for inclusion in Masters Theses by an authorized administrator of TRACE: Tennessee Research and Creative Exchange. For more information, please contact trace@utk.edu.

To the Graduate Council:

I am submitting herewith a thesis written by Jeremy Bryant Campbell entitled "A Two-Phase Cooling Method Using R134a Refrigerant to Cool Power Electronics Devices." I have examined the final electronic copy of this thesis for form and content and recommend that it be accepted in partial fulfillment of the requirements for the degree of Master of Science, with a major in Electrical Engineering.

Leon M. Tolbert, Major Professor

We have read this thesis and recommend its acceptance:

Jack Lawler, Syed K. Islam

Accepted for the Council:
Carolyn R. Hodges

Vice Provost and Dean of the Graduate School

(Original signatures are on file with official student records.)

To the Graduate Council:

I am submitting herewith a thesis written by Jeremy Bryant Campbell entitled "A Two-Phase Cooling Method Using R134a Refrigerant to Cool Power Electronics Devices." I have examined the final electronic copy of this thesis for form and content and recommend that it be accepted in partial fulfillment of the requirements for the degree of Master of Science, with a major in Electrical Engineering.

Leon M. Tolbert

Major Professor

We have read this thesis
and recommend its acceptance:

Jack Lawler

Syed K. Islam

Accepted for the Council:

Anne Mayhew

Vice Chancellor and
Dean of Graduate Studies

(Original signatures are on file with official student records.)

A Two-Phase Cooling Method Using R134a Refrigerant to Cool Power Electronics Devices

A Thesis

Presented for the

Masters of Science

Degree

The University of Tennessee, Knoxville

Jeremy Bryant Campbell

December 2004

Copyright © 2004 by Jeremy B. Campbell

All rights reserved.

Dedication

This thesis is dedicated to my family

Roger L. Campbell

Charlotte V. McKinney

Julie A. Britt and family

Jeffrey L. Campbell and family

Dad, I know you are looking down, and watching over us; we miss you!

Mom, Julie, and Jeff, Thank You for all the prayers, encouragement, and support.

Acknowledgements

I would like to thank many people who supported me in finishing this thesis. First and foremost, I would like to thank my advisor, Dr. Leon M. Tolbert for opening more doors than I ever dreamt possible; also for your advice and genuine concern for all your students.

I would like to thank my committee members, Drs. Jack Lawler and Syed K. Islam.

I would like to acknowledge Donald J. Adams for the opportunity to work at Oak Ridge National Laboratory. I would also like to thank Curtis Ayers, Burak Ozpineci, Madhu Chinthavali, Chester Coomer, and the PEEMRC team for their valuable support.

I would like to especially thank Tony Zeind for his unwavering friendship. I would not be here without your pep talks.

A special thanks to all my fellow colleagues at The University of Tennessee.

Abstract

Power electronics are vital to the operation and performance of hybrid-electric vehicles (HEVs) because they provide the interface between the energy sources and the traction drive motor. As with any "real" system, power electronic devices have losses in the form of heat energy during normal switching operation, which has the potential ability to damage or destroy the device. Thus, to maintain reliability of the PE system, the heat energy produced must be removed. Present HEV cooling methods provide adequate cooling effects, but lack sufficient junction temperature control to maintain long-term reliability. This thesis is based on using the automobile's air conditioning system as an alternative to conventional power electronics cooling methods for hybrid-electric vehicle applications.

This thesis describes the results from a series of experiments performed on a circuit containing an IGBT, gate controller card, and snubber while submerged in an automotive refrigerant bath (R134a). The circuit was then tested while being cooled using a mock automotive air conditioning system. Tests were performed on custom made thin-film resistors while being cooled by the same mock air conditioning system. The thin-film resistors were arranged to resemble a six-switch, three-phase inverter in steady-state operation. Lastly, an active IGBT junction cooling technique is described and simulated, which incorporates direct cooling of the junction of the power electronic device rather than its case. The results from the simulation indicate the exposed junction IGBT technique would benefit the device by reducing the junction temperature, increasing forward current ratings, and increasing reliability.

Table of Contents

CHAPTER 1 .... **1**

INTRODUCTION 1
1.1 TRANSPORTATION REQUIREMENTS 2
1.2 POWER ELECTRONICS IN HEVS 4
1.3 HISTORY OF REFRIGERATION 6
1.4 REFRIGERATION PROCESS 7
1.5 OUTLINE OF THESIS 8

CHAPTER 2 .... **10**

HEAT SINK TECHNOLOGY 10
2.1 SEMICONDUCTOR THERMAL MODEL 11
2.2 POWER ELECTRONICS COOLING METHODS 12
2.2.1 Natural Convection 13
2.2.2 Forced-Convection 16
2.2.3 Liquid Cooled 18
2.2.4 Pool Boiling 20
2.3 POWER ELECTRONICS COOLED BY R134A REFRIGERANT 23

CHAPTER 3 .... **24**

EXPERIMENTAL RESULTS 24
3.1 LOSSES IN POWER ELECTRONICS 24
3.1.1 Conduction Losses 27
3.1.1.1 Piece-Wise Linear (PWL) Model 29
3.1.1.2 Calculating Conduction Losses 30
3.1.2 PWL Experimental Results 30
3.1.3 Switching Losses 33
3.2 EXPERIMENTAL RESULTS OF POWER DISSIPATION 34
3.2.1 Air Cooled and R134a Cooled Experimental Results 34
3.2.2 Automotive R134a Air Conditioner System Results 40
3.3 SUMMARY 47

CHAPTER 4 .... **48**

SYSTEMS AND SIMULATION 48
4.1 THREE-PHASE INVERTER 48
4.2 THIN-FILM RESISTOR 51
4.2.1 Thin-Film Resistor Extrapolation 56
4.3 ACTIVE IGBT JUNCTION COOLING SIMULATION 58
4.3.1 Single IGBT Simulation 59
4.4 SUMMARY 62

CHAPTER 5 .... **64**

CONCLUSION AND FUTURE WORK 64

5.1 CONCLUSION 64
5.2 FUTURE WORK 65

LIST OF REFERENCES 67

APPENDICES 70

APPENDIX I 71

APPENDIX II 79

APPENDIX III 80

VITA 81

List of Tables

Table **Page**

3.1 TEMPERATURE DEPENDANT R_D AND V_D RESULTS OF THE IGBT TESTED…..…...32

3.2 POWER DISSIPATED FROM TESTED IGBT AND PWL COMPARISON...…………....40

3.3 EFFICIENCY OF IGBT..……………………………………………….…………...46

4.1 THIN-FILM RESISTOR EXPERIMENTAL RESULTS.………...……….…………….....54

4.2 EXTRAPOLATED THIN-FILM RESISTOR RESULTS.…………………………………56

List of Figures

Figure **Page**

1.1 HEV ENERGY DISTRIBUTION SYSTEM CONFIGURATION…...……………………...5

1.2 DIAGRAM OF AIR CONDITIONER COMPONENTS…..………………………………..8

2.1 SEMICONDUCTOR THERMAL MODEL (A) HEAT ENERGY FLOW IN PE DEVICES (B) STEADY-STATE THERMAL CIRCUIT…….….……………………………….………...12

2.2 SELECTION OF NATURAL CONVECTION HEAT SINKS…….………………….…15

2.3 HIGH POWER, THREE-FAN, FORCED-CONVECTION HEAT SINK.…………………..17

2.4 LINEAR AND IMPINGEMENT AIRFLOW….…………………………………………17

2.5 LIQUID COOLED HEAT SINK….…………………………………………………..20

2.6 POOL BOILING TECHNIQUE………………..…………………………………...21

3.1 CONTROLLABLE SEMICONDUCTOR SWITCHING CHARACTERISTICS….…………...25

3.2 *I-V* CHARACTERISTICS (A) TYPICAL DIODE (B) TESTED IGBT....………………...28

3.3 PWL DIODE MODEL (A) DIODE SYMBOL AND PWL MODEL (B) *I-V* CURVE OF THE PWL MODEL………………………………………………………………..29

3.4 TEMPERATURE DEPENDANT *I-V* CURVES OF THE IGBT TESTED……...…………..31

3.5 PWL MODEL PARAMETERS VERSUS TEMPERATURE (A) R_D VS. T (B) V_D VS. T….33

3.6 EXPERIMENTAL CIRCUIT..…………………………………………………...35

3.7 EXPERIMENTAL R134A SYSTEM (A) SUBMERGED IGBT COOLING TECHNIQUE (B) TEST VESSEL INCLUDING PE CIRCUIT………..…………………………………...36

3.8 EXPERIMENTAL CIRCUIT CONTAINING POWER ANALYZER AND CONNECTIONS.…37

Figure		Page

3.9 EXPERIMENTAL RESULTS FOR R134A-COOLED AND AIR-COOLED POWER SYSTEMS (A) VOLTAGE WAVEFORMS (B) CURRENT WAVEFORMS (C) EXPANDED VOLTAGE AND CURRENT TURN-OFF WAVEFORMS (D) INSTANTANEOUS AND AVERAGE POWER LOSS……………………………………………………………..………….39

3.10 MOCK AUTOMOTIVE AIR CONDITIONER SYSTEM WITH VESSEL AND CIRCUIT…...41

3.11 TEMPERATURE OF AMBIENT VERSUS TIME FROM REFRIGERATION TEST...………44

3.12 INSTANTANEOUS VOLTAGE, CURRENT, AND POWER WAVEFORMS FROM AUTOMOTIVE AIR CONDITIONER SYSTEM COOLING IGBT (A) 6 A TEST (B) 7 A TEST (C) 8 A TEST (D) 9 A TEST……………………………………………...45

4.1 THREE-PHASE INVERTER DRIVING AN AC MACHINE……………………………..49

4.2 CHARACTERISTIC WAVEFORMS FOR THREE-PHASE INVERTER (A) CARRIER TRIANGLE WAVE AND CONTROL WAVEFORMS (B) V_{an} OUTPUT WAVEFORM (C) V_{bn} OUTPUT WAVEFORM (D) V_{ab} OUTPUT WAVEFORM…….……………………………50

4.3 THIN-FILM RESISTER CIRCUIT (A) CIRCUIT DIAGRAM (B) RESISTOR ASSEMBLY....53

4.4 RESISTOR TEMPERATURE AND POWER DISSIPATION VERSUS TIME……….……...54

4.5 EXTRAPOLATED TEMPERATURE VERSUS AVERAGE FORWARD CURRENT CURVES (A) CENTER BRANCH (B) RIGHT BRANCH (C) LEFT BRANCH (D) BULK REFRIGERANT……………………………………………………………………….57

4.6 AVERAGE POWER DISSIPATED VERSUS FORWARD CURRENT……………………60

4.7 THERMAL MODEL (A) IGBT WITH CASE (B) IGBT WITH EXPOSED JUNCTION…...61

4.8 JUNCTION TEMPERATURE VERSUS FORWARD CURRENT…………………………62

A.1 TEMPERATURE RECORDER PROGRAM USER INTERFACE……………………….…80

Chapter 1

INTRODUCTION

Electric cars have been an option since the beginning of the automobile revolution. Early electric vehicles were mechanically robust, but lacking horsepower because of poor battery technology. Thus, the internal combustion (IC) engine quickly became the best power plant for the automobile because petroleum fuel was a superior source of energy. Petroleum fuel was chosen due to its high-energy density properties, ease of handling, and cheap abundant supplies.

Today, more than 100 years later, cities have become choked with combustion by-products of petroleum, and the world's dependence on petroleum continues to increase, while petroleum deposits are diminishing. Consequently, these concerns are renewing interest for alternative energy sources in the transportation industry. While there are many options, the electric and hybrid electric vehicles (EV/HEV) are the most promising alternatives to the IC powertrain as these options maintain the automotive industry, which helps the world's economy thrive. This renewed interest has recently spurred the Toyota Prius™ and Honda Insight™. These HEVs are the first HEVs to make production.

Power electronics (PEs) are vital to the operation and performance of EVs and HEVs. Power electronics provide the interface between the energy sources such as batteries and the traction drive motor. PEs must meet strict automobile manufacturers' design criteria when used in EVs and HEVs. The four most import design criteria for the automotive industry are weight, size, reliability, and cost.

The thermal management system for power electronics devices plays an important role in all four design criteria. PEs capabilities are highly temperature dependent. To maintain reliability of PE systems, the temperature must be strictly regulated. If the temperature is allowed to vary, the PE devices must be oversized for their typical application in order to meet every operating condition. Existing thermal management designs rely mainly upon oversizing the PEs as just described or by inclusion of large heat sinks, both of which detract from the size and cost criteria of automotive design criteria. Present thermal management techniques for power electronics cannot meet all the requirements of the transportation industry. However, existing air-conditioning (A/C) systems in automobiles with little modification can be used to cool PE devices. Utilization of the existing A/C systems to directly cool the PEs can help meet the design criteria described previously.

This thesis describes a new technique of directly submerging PEs in a vehicle's refrigerant (R134a) as an active method to cool power electronic devices. This technique is shown to meet the demanding requirements of the automotive industry. This technique will be discussed in the next sections with specific application to the HEV systems.

1.1 Transportation Requirements

In an effort to increase HEV development, the United States Department of Energy (DOE) has partnered with automotive manufacturers, universities, national laboratories, and various industry leaders in a program called the FreedomCAR (Cooperative Automotive Research). The goal of this partnership is to share technology in an effort to

develop more energy efficient and environmentally friendly highway transportation technologies. In turn, the transportation industry will provide these technologies to the consumers in the least amount of time. To meet these goals, the technology must first be developed. Outlining the efforts for the FreedomCAR partners are the following design requirements:

- Electric propulsion systems, electric motor and inverter, with a 15-year life capable of delivering at least 55 kW of power for 18 seconds and 30 kW of continuous power at a system cost of $12/kW peak.
- Electric propulsion system having a coolant inlet temperature of 105ºC.
- Electric drivetrain energy storage with a 15-year life with discharge power of 25 kW for 18 seconds and $20/kW.
- Material and manufacturing technologies for high-volume production vehicles that provides 50% reduction in the weight of vehicle structure and subsystems, affordably, and increased use of recyclable/renewable materials.

Thermal management technology of power electronics devices has a direct impact on all the above design requirements. An effective, small, lightweight thermal management system will contribute to greater efficiency and reliability of the power electronics devices. In turn, a lighter vehicle results in less demand on the engine and/or motor, faster acceleration, and greater energy efficiency. Higher energy efficiency contributes to less fuel or battery consumption.

1.2 Power Electronics in HEVs

Simplistically, power electronics are responsible for the process and controlled flow of electric energy by supplying voltages and currents in a form that is optimally suited for user loads [1]. In HEVs, PEs are the interface between the energy sources and the traction drive motor for both power consumption and regenerative cases. Figure 1.1 shows a HEV's typical configuration. As shown in the figure, PEs allow the HEV to operate as they connect the batteries to the motor and generator (in some cases these may be the same devices) allowing the vehicle to function.

Driving conditions vary from flat interstate cruising to start and stop city driving. The most severe driving conditions require hard acceleration and braking. These conditions force power electronics to their extreme limits such that they must conduct high forward biased currents, block high forward and reverse voltages, cycle on and off within microseconds, and resist thermal breakdown because of external environmental conditions and their own internally produced heat.

Severe driving conditions can force the traction motors to exceed 100 Amps peak and 80 Amps continuous. The forward and reverse voltage blocking capabilities of PEs can greatly exceed 300 Volts; yet using PEs with higher voltage blocking capabilities will minimize the need to configure multiple devices in series, thus lowering on-state voltages and conduction losses. PE devices must also be required to have fast turn-on and turn-off transitions, yet they must have small dv/dt and di/dt to minimize switching losses. An increase in switching cycles will increase power losses.

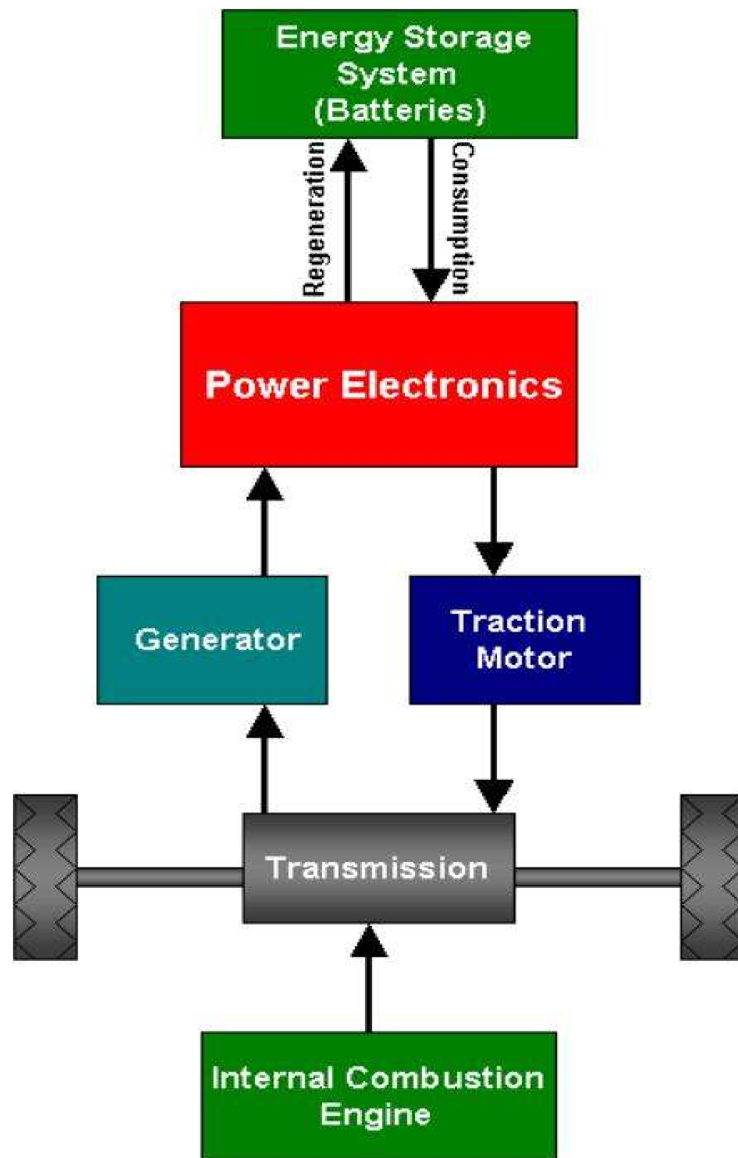

Figure 1.1. HEV energy distribution system configuration

Traditional automobiles as well as HEVs produce temperatures over 105°C in the engine compartment due mainly to the IC engine heat dissipation. Unfortunately, this is the ideal physical location for most power electronics devices as it offers some environmental protection (rain, debris, etc), space for mounting, minimizes stray inductance, and is the location of existing A/C systems thus helping to minimize the additional PE load to A/C system.

1.3 History of Refrigeration

The definition of air conditioning is the control of temperature, humidity, purity, and motion of air in an enclosed space, independent of outside air conditions [2]. Refrigeration or air conditioning was first widely introduced in the late 1800s in the form of household refrigerators for food product storage. Soon air conditioning usage was expanded to cooling homes and business. Eventually in the 1950s, automobiles started becoming equipped with A/C systems. Today, nearly all of new automobiles sold in the US are equipped with an A/C system, becoming more of a standard rather than a luxury.

The first refrigerators began by using a toxic mixture of refrigerant that included ammonia (NH_3) and methyl chloride (CH_3Cl). This mixture is toxic to people if the system were to leak, so in 1928, a non-toxic replacement refrigerant called Freon was invented. However, the Environmental Protection Agency (EPA) has determined that chlorofluorocarbons (CFCs) based refrigerants such as Freon, are harmful to the environment. It was determined that these refrigerants are a major contributor to the depletion of the earth's ozone layer. The "Montreal Protocol," an international

agreement, established a plan to reduce emissions of CFCs and was signed by a total of 24 nations in September of 1987. Since 1993, Tetrafluoroethane (R134a) has become the environmentally friendly replacement to Freon in automobiles. R134a's prevalent usage in A/C systems and ideal thermal properties makes it ideal for use as an active coolant for PE devices in HEV applications.

1.4 Refrigeration Process

Refrigeration is based upon exploiting the evaporation process. When a liquid evaporates, it absorbs heat from its surrounds, thus reducing the surrounding temperature. Active A/C systems, such as the one in an automobile's A/C system, extend this process to include a self-contained, re-circulating refrigerant system. Figure 1.2 is a block diagram of the automobile's refrigeration process. The process begins at the compressor where it compresses R134a refrigerant from a low pressure cool gas to a high pressure hot gas (vapor). The hot vapor flows through coils called a condenser to condense the vapor to a liquid by dissipating the heat in the hot gas. The liquid travels through an expansion valve, and in the process, the liquid changes pressure to become a cold low pressure liquid. The low pressure liquid flows through another set of coils called an evaporator that allows the vapor to absorb heat. The absorbed heat is derived from standard automotive cabin load.

With little modification to existing automobile A/C systems, it can be used to cool power electronics. It is desirable to modify the system by adding the PEs at the evaporator because the refrigerant is at its coldest liquid state. The modifications to

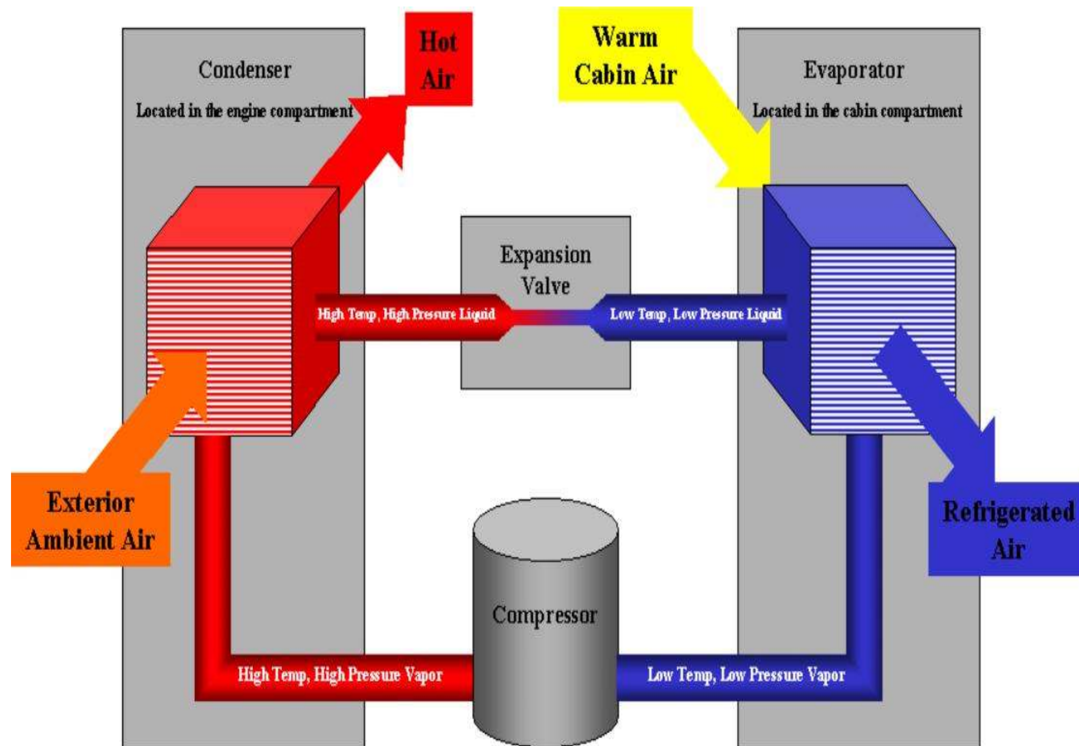

Figure 1.2. Diagram of air conditioner components

existing automotive A/C systems would require two extra refrigerant tubes and a pressure vessel to hold the PEs. One tube is used to divert the liquid refrigerant to the vessel containing the power electronics equipment, and the second tube is used as a return. Automobile manufacturers will benefit from this approach by reducing cost and weight of the vehicle.

1.5 Outline of Thesis

The objective of this thesis is to investigate and evaluate a two-phase cooling method using R134a refrigerant to dissipate the heat energy generated by the rectifiers, converters, and inverters of PEs used in HEV application.

First, a silicon IGBT current vs. voltage characteristics will be modeled. Then, an evaluation of the IGBT submerged in R134a to identify advantages of the proposed cooling method over conventional cooling methods will be conducted. Last, a system study of an inverter cooled by a vehicle's air conditioning system is conducted to provide an increase in energy efficiency and reliability.

Chapter 2 is a summary of existing thermal management techniques with several examples.

Chapter 3 explains the approach used to characterize and model the IGBT, evaluate power dissipation, and study the effects R134a refrigerant on power electronics devices.

Chapter 4 discusses the thermal model and applies it to an automotive application.

Chapter 5 provides conclusions and recommendations.

Chapter 2

HEAT SINK TECHNOLOGY

In past years, electrical devices that delivered significant levels of power were typically packaged with large enclosures to house large heat sinks or base plates. No formal method, other than experience, was widely used for predicting the size of the heat sink required to maintain a particular device temperature and operating life. Consequently, the solution to maintain an operating temperature became one of using the largest heat sink and enclosure, a brute force solution. While this method is adequate for previous PE generations, present day power electronics are smaller, conduct more current, and generate larger heat densities, where the current cooling requirements are more complex and cannot generally be solved with a simple aluminum mass.

This chapter begins by establishing a semiconductor thermal model where heat energy is calculated by formulas similar to Ohm's Law. The remainder of the chapter is dedicated to four thermal management systems commonly used by engineers today. These include natural convection, forced-convection, liquid cooled, and pool boiling. Each system has their own set of advantages and disadvantages all of which will be explored in some detail.

2.1 Semiconductor Thermal Model

When a section of material has a temperature difference across the surface, there is a net flow of energy from the higher temperature surface to the lower temperature surface. The energy flow per unit time or power is given by:

$$P = \frac{\lambda A \Delta T}{d} \tag{2.1}$$

where $\Delta T = T_2 - T_1$ is in °C, A is the across-sectional area in m^2, d is the length in meters, and λ is the thermal conductivity in W-m^{-1} °C^{-1}. Thermal conductivity is a measurement that yields a material's ability to conduct heat given the amount of heat energy, in watts, per given distance, in meters, and change in temperature, in °C. For 90% aluminum, which is typically used for heat sinks, the thermal conductivity is 220 W-m^{-1} °C^{-1} [1].

The concept of energy flow can be equivalent to circuit analysis by introducing an analogy of terms. Ohm's Law states an electrical voltage V is proportional to the product of current I and resistance R. In the thermal circuit, a difference in temperature ΔT is viewed as a voltage drop V, the power dissipated P is viewed as a current I, and thermal resistance R_θ as electrical resistance R. The thermal circuit equation takes the form:

$$\Delta T = P R_\theta \tag{2.2}$$

The thermal characteristics of a semiconductor can also be modeled by the thermal circuit equation [3]. Shown in figure 2.1(a), the thermal circuit model identifies four different materials, each having different thermal conductivity and temperatures between each section, including junction to ambient. Figure 2.1(b) is an equivalent steady-state thermal circuit for the semiconductor model. Based on the thermal circuit,

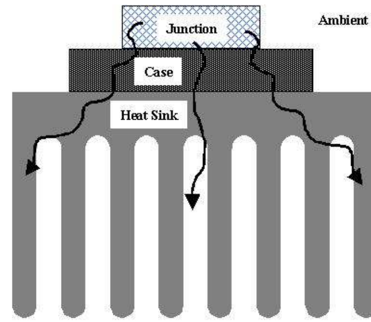

(a)

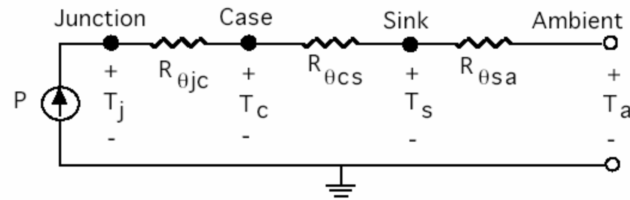

(b)

Figure 2.1. Semiconductor thermal model **(a)** Heat energy flow in PE devices **(b)** Steady-state thermal circuit

equation 2.3 solves for the temperature of the junction T_j, where the resistances of the junction, case, sink, ambient temperature, and the total power dissipated ($R_{\theta jc}$, $R_{\theta cs}$, $R_{\theta sa}$, T_a and P_{total} respectively) are given, then:

$$T_j = P_{total}\left(R_{\theta jc} + R_{\theta cs} + R_{\theta sa}\right) + T_a \tag{2.3}$$

2.2 Power Electronics Cooling Methods

Device junction temperature, ambient air temperature, enclosure size, and system cost are a few thermal management challenges facing engineers. Manufacturers provide a wide variety of solutions for thermal management systems that assist engineers. This

section will investigate four of the most popular among industry, then comment on each system's advantages and disadvantages for HEV applications.

2.2.1 Natural Convection

Natural convection or air-cooling is still widely used, and will always be favored whenever possible, as it is the least expensive of all cooling systems [4]. However, directly cooling PEs by mere ambient air alone is typically not enough to keep the junction temperature below the manufacturer's recommended level. Thus, PEs must be mounted on heat sinks, typically aluminum. Aluminum provides adequate thermal conductivity, reduced weight, and reduced cost when compared to materials such copper or steel [5].

There are two main parts that comprise a heat sink, base plate and fins. The base plate has three responsibilities:

1. Provide a surface where the PE devices are attached
2. Structural rigidity to the system
3. Spread heat away from the PE to the fins.

Engineers must compromise between the proper heat spreading and conduction losses within the base plate. A base plate that is too thick will have minimum conduction losses, but heat spreading in the lateral direction will decrease, resulting in a lower system thermal efficiency and excessive weight. A base plate too thin will obtain an increase in heat spreading, but an increase in conduction losses and lack the structural rigidity need for self support and support for mounted PEs. The optimum base plate

thickness is governed by the number of PE devices, the surface area covered by each device, the mechanical requirements for device mounting, and the circuit application. A circuit application in steady-state mode is cooled best with a thin base plate and a large number of fins along the width, while a circuit application in impulse mode is cooled best with a thicker base plate and reduced amount of fins across the width [5].

Fins are constructed of thin vertical plates of metal welded or machined to the base plate and provide deep channels for an increase in surface area to assist convective cooling. The fins have constraints for height and spacing, where altering one will cause the performance of the fin to change. Increasing the height of the fin beyond the point where the fin temperature reaches ambient temperature provides no useful purpose. Fin spacing determines the airflow across the fin surface. Movement of air molecules by natural convection is induced when a surface is at an elevated temperature above ambient. Then as air molecules pass by the fin surface, heat energy is transferred to the air. As fin spacing decreases, less air can pass across the fin surface and no heat energy is transferred. On the other hand, as the fin spacing increases, fewer fins exist, thus reducing the convective heat transfer.

Additional advantages of natural convection heat sinks are no moving parts and a large selection from manufacturers. No moving parts greatly increase reliability and reduce cost of the cooling system. Multiple options exist for most power levels and enclosure types giving design engineers flexibility to choose a heat sink that best fits their design application. Figure 2.2 is an example of 12 different natural convection heat sinks including a table of corresponding thermal resistance and volume specifications for each. The thermal resistance $R_{\theta sa}$ measured in °C/W is the theoretical resistance between the

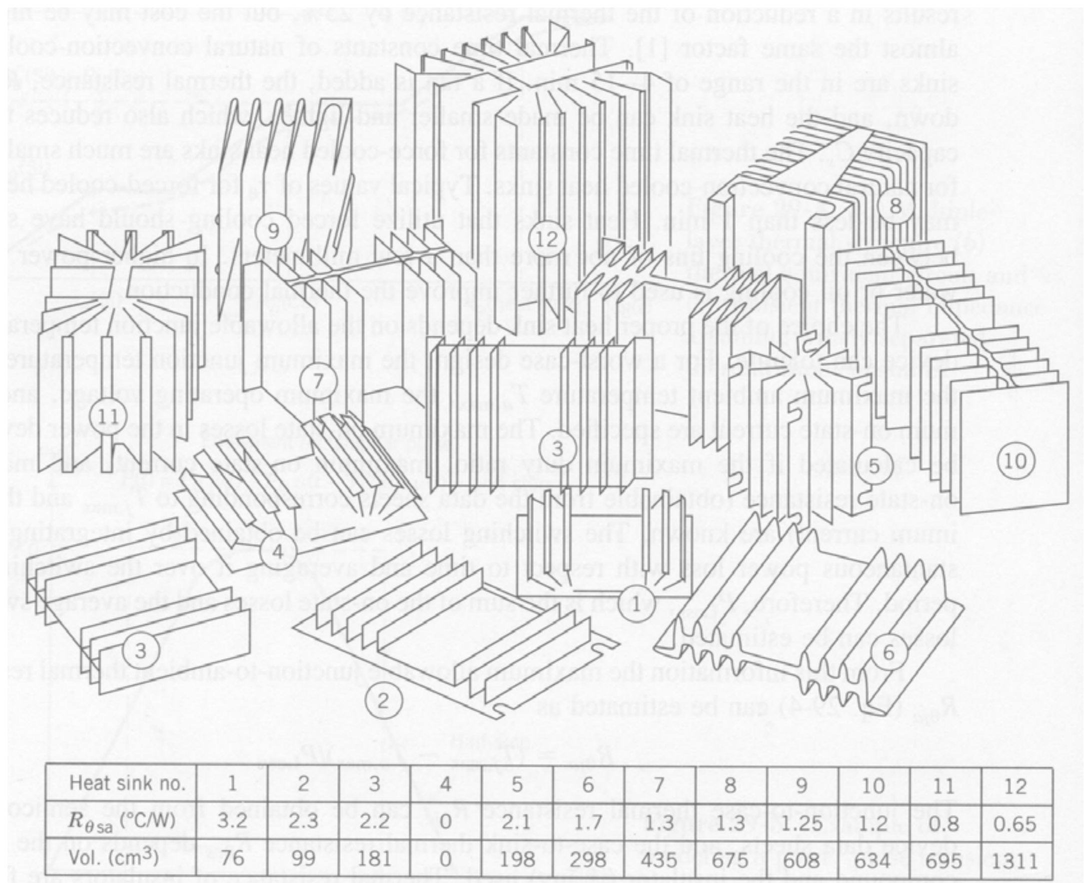

Heat sink no.	1	2	3	4	5	6	7	8	9	10	11	12
$R_{\theta sa}$ (°C/W)	3.2	2.3	2.2	0	2.1	1.7	1.3	1.3	1.25	1.2	0.8	0.65
Vol. (cm^3)	76	99	181	0	198	298	435	675	608	634	695	1311

Figure 2.2. Selection of natural convection heat sinks [1]

heat sink and the ambient air, which determines how much heat energy is dissipated to the ambient air. The volume of each heat sink is measured in cm^3, and this measurement is used to determine the enclosure requirements.

Engineers must keep in mind that the cooling capability of natural convection heat sinks is heavily dependant upon the ambient temperature and a clean fin surface. Dirt, dust, and related matter can also deteriorate the heat sink's cooling capability by retaining excessive heat energy and increasing the thermal resistance R_{sa}. As the surrounding air temperature increases, the cooling capability decreases, because less heat can be absorbed by the surrounding environment. R-theta® designs all natural convection heat sinks for optimum performance at 50°C above ambient [5].

2.2.2 Forced-Convection

Because air has such poor thermal transport properties, forced circulation is often required to enhance the heat dissipation process in natural convection heat sinks [4]. Air is forced across the fin surface by use of a fan. This lowers the thermal resistance $R_{\theta sa}$ and enables the heat sink to disperse more heat. Forced-convection heat sinks can provide 20 W/cm^2 [6]. Figure 2.3 is a high power, three-fan, forced-convection heat sink. The fan can be designed into one of two arrangements, linear and impingement air flow, shown in figure 2.4. The linear air flow is designed to push or pull air across the surface of the fins. A pushing air system is used more frequently because cool, fresh air is drawn through the fan resulting in less wear on bearings; however, there is no difference in heat sink cooling capability between linear push and pull. The impingement air flow design can reduce the heat sink size by 50% when compared to the linear air flow, because the

Figure 2.3. High power, three-fan, forced-convection heat sink

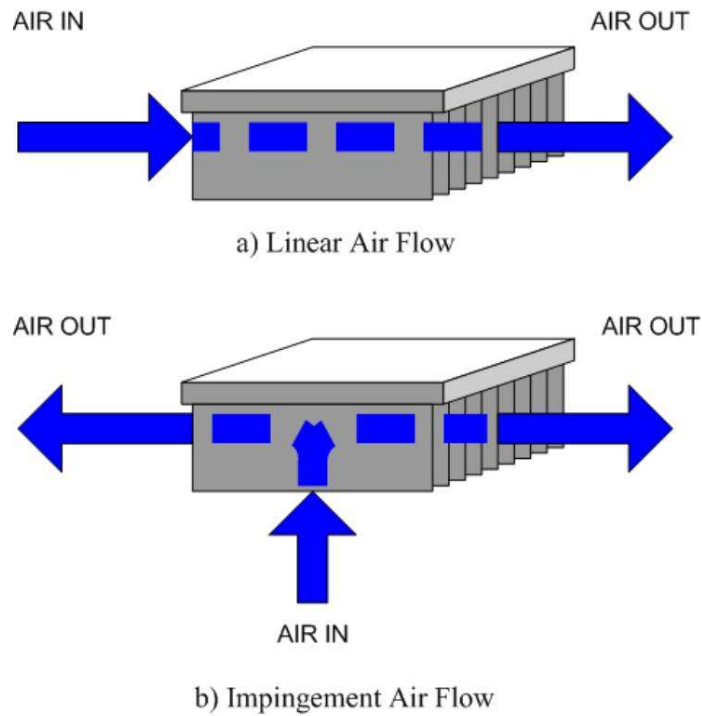

Figure 2.4. Linear and impingement airflow [5]

free air area of the fin is doubled [5]. By design, the air in the impingement air flow system has a shorter distance to travel and a larger volume of flow resulting in a lower temperature difference between a fin's beginning (side closest to the air in) and end (side closest to the air out) [7].

The advantages of forced-convection heat sinks are smaller size, lighter weight, and more efficient compared to natural convection heat sinks. These advantages enable engineers to design PEs to be placed in smaller enclosures, which reduce the system's overall size, weight, and possibly the cost. The fan is usually a low current device drawing no more than 0.25 A and 30 W, which is only a fraction of the total power dissipated by the heat sink.

Natural convection and forced-convection heat sinks are not capable of meeting HEV demands on power electronics [8]. Excessive ambient temperatures and dirty conditions in the engine compartment will likely cause a decrease in efficiency and ultimately lead to the premature failure of the PE devices. Also, any air-cooled heat sink designed for HEV application would require an excessive mass of aluminum, much larger and heavier than an HEV application could conveniently accept.

2.2.3 Liquid Cooled

Liquid cooling is designed to exploit the excellent thermal conductivity properties of liquids such as water and ethylene glycol known as coolants. The thermal conductivity of water is 0.60 $W\text{-}m^{-1}K^{-1}$, which makes it one of the best thermal conductors among all liquids. Unfortunately, water has poor dielectric characteristics that contribute to short circuits and electrical equipment failure.

Traditionally, the solution to separating the liquid from the electrical devices is to contain the liquid in a closed loop system, where the liquid does not contact the device, but rather the substrate upon which the device is mounted. The components needed for liquid cooling are comprised of a heat sink, piping, liquid pump, and a condenser. A liquid cooled heat sink differs from an air cooled heat sink in the construction. The liquid cooled heat sink has cavities that channels water through the heat sink, absorbing the sink's heat, and then discharging the water without the liquid physically contacting the device.

The process of liquid cooling PEs, shown in Figure 2.5, involves a coolant entering the heat sink, which houses the semiconductors. Heat is conducted away from the semiconductor through the heat sink and absorbed by the coolant. Then, the coolant travels out of the heat sink through a pipe, and enters the condenser. Last, the hot coolant travels through the condenser where the heat from the water is dissipated to the surrounding air, before being cycled through the entire system repetitively.

Liquid cooling reduces the thermal resistance between the semiconductor case and ambient air, implying a greater heat transfer. Heat flux of 100 W/cm2 can be achieved, well beyond the ability of forced-air heat sinks [6]. Presently, HEVs use a liquid cooled heat sink with an ethylene glycol based coolant [9,10]. Based on FreedomCAR requirements for maximum liquid temperature of 105°C, the coolant loop is separate from the liquid loop used to cool the IC engine.

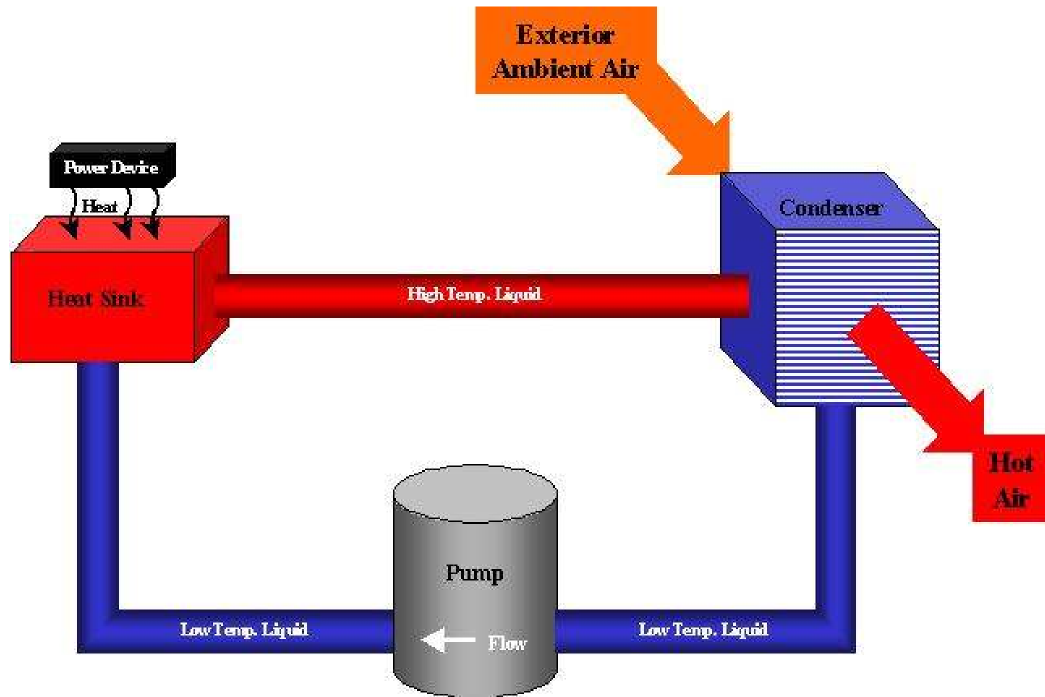

Figure 2.5. Liquid cooled heat sink

The major disadvantage of liquid cooling in HEVs is in power electronics reliability. Liquid temperatures above 105°C lower PE reliability significantly, because the PEs are operating at temperatures 20°C above the recommended temperature for best reliability [4,11]. As a rule of thumb, the failure rate for semiconductors devices doubles for each 10-15°C temperature rise above 50°C [1]. Another disadvantage in using a separate coolant loop is an increase in vehicle weight from the additional components of the separate loop such as coolant and coolant hoses, pump, and a radiator.

2.2.4 Pool Boiling

Another technique of liquid cooling is pool boiling, where the coolant is in direct contact with the semiconductor. Pool boiling requires a liquid with high dielectric

properties, because the fluid will flood the spaces around the semiconductor, and inherently, become in contact will electrical current. The fluid must be an electrical insulator.

The pool boiling cooling system relies upon the passive circulation of the dielectric fluid inside a sealed chamber. Figure 2.6 shows heat generated by the semiconductor is dissipated to the dielectric liquid, which boils and produces vapor bubbles. The bubbles are driven by buoyancy into the upper region of the chamber. The vapor condenses on the surfaces of the vessel to form liquid droplets, which returns to the liquid pool. The vessel dissipates the heat energy to the ambient air by external fins and in some cases forced air.

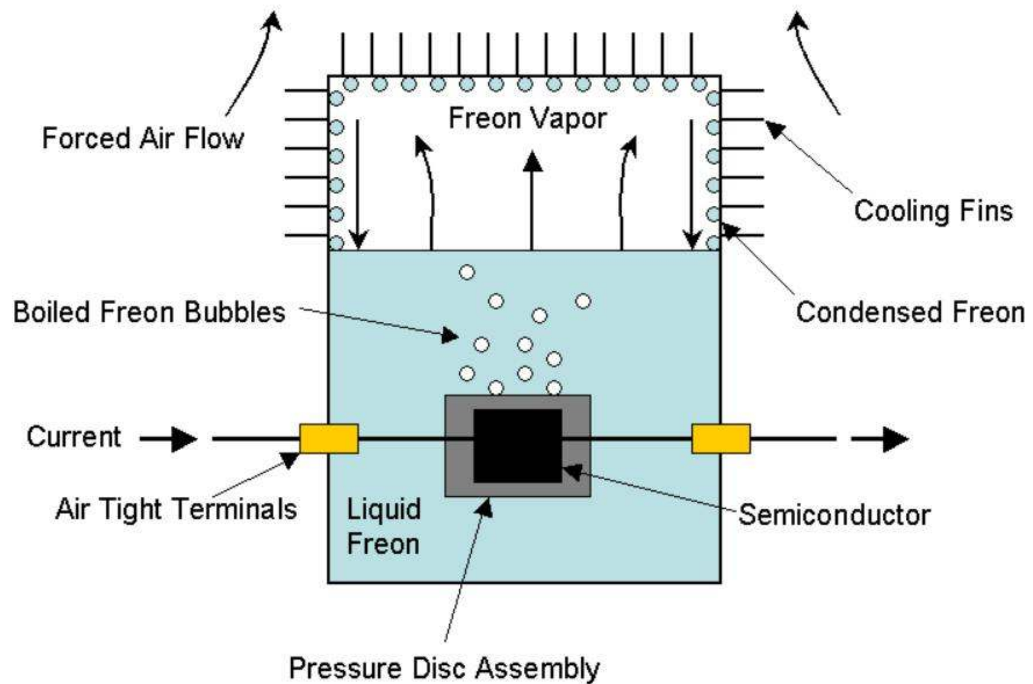

Figure 2.6. Pool boiling technique [12]

Pool boiling is one of the most efficient techniques to remove heat from a device [13]. Heat flux for pool boiling can exceed 100 W/cm^2; at this rate, more heat energy can be dissipated in less area than any previous thermal management techniques discussed previously [6]. Additional advantages of pool boiling include a decrease in the size and weight of the cooling system, and the PEs are isolated from external contaminants such as dust and dirt as this too is a closed system [12,14].

The disadvantages of employing pool boiling cooling systems to an HEV application include a limited selection of dielectric fluids and contamination collection on vessel cooling fins from the engine compartment. Intimate contact of the liquid with the device places stringent chemical and electrical compatibility constraints, limiting the choice of coolant to a select few. One choice is CFCs based refrigerants; however, these fluids are harmful to the environment and are banned by governmental laws. Another choice for a dielectric fluid is FC-72, more commonly known as Fluorinert. Fluorinert is manufactured by the 3M™ company, and designed to be a pool boiling refrigerant. It possesses high dielectric characteristics and has similar thermal conductivity characteristics to CFCs based refrigerants [11,12]. Additional fluids exist yet fail to be successful enough to be considered.

Pool boiling cooling systems containing CFCs based refrigerants were used in traction drive and various motor drives applications before the governmental ban [12,14]. Pool boiling cooling systems containing Fluorinert are currently in development for high power electronic chip applications [4,6,13].

2.3 Power Electronics Cooled By R134a Refrigerant

In the next chapter, cooling power electronic devices by submerging the devices in R134a refrigerant is considered. Experimental tests on a submerged and air-cooled IGBT and gate-controller card to study the R134a dielectric characteristics, deterioration effects, and heat flux capacity are conducted and results are presented.

Chapter 3

EXPERIMENTAL RESULTS

Power electronics devices inherently produce losses during conduction, blocking, and switching cycles. Semiconductors that generate more heat than is properly dissipated will have reduced reliability, increased failure, and damage may possibly spread to other equipment. Therefore, engineers must prevent failure by understanding how semiconductor losses are generated. This chapter begins with a study of semiconductor losses, and then continues with experimental tests that determine losses in air-cooled and R134a-cooled environments, during an extended soak for more than 300 days were performed on a submerged IGBT and gate-controller card to study the R134a dielectric characteristics and deterioration effects. Additionally, a mock automotive air conditioner system was used to cool the IGBT similar to an HEV application. The results from these tests are presented in this chapter.

3.1 Losses in Power Electronics

Silicon (Si) based power electronics devices are based on four states of operation, which includes conduction, blocking, turn-on, and turn-off. Conduction is the time period in which forward current passes through the device. Blocking is the time period in which little current flows and full voltage is across the device. Between the conduction and blocking states, the turn-on and turn-off transitions exist. By design, the turn-on and

turn-off transition periods are on the order of 1000 times shorter in comparison to the conduction or blocking time periods.

An ideal power electronic device would be one that conducts large forward currents with no voltage drop, blocks large forward and reverse voltages with no current flow, and transitions on-to-off or vise-versa instantaneously when triggered. Unfortunately, physical Si devices do not have these ideal characteristics, so they dissipate energy in the form of heat during these four states of operation. Figure 3.1 plots instantaneous voltage, current, and energy dissipation (loss) waveforms during one cycle in a typical semiconductor. In Figure 3.1, the instantaneous power peaks during the turn-on and turn-off periods, while only a small amount of instantaneous power is dissipated during the conduction and blocking periods [1].

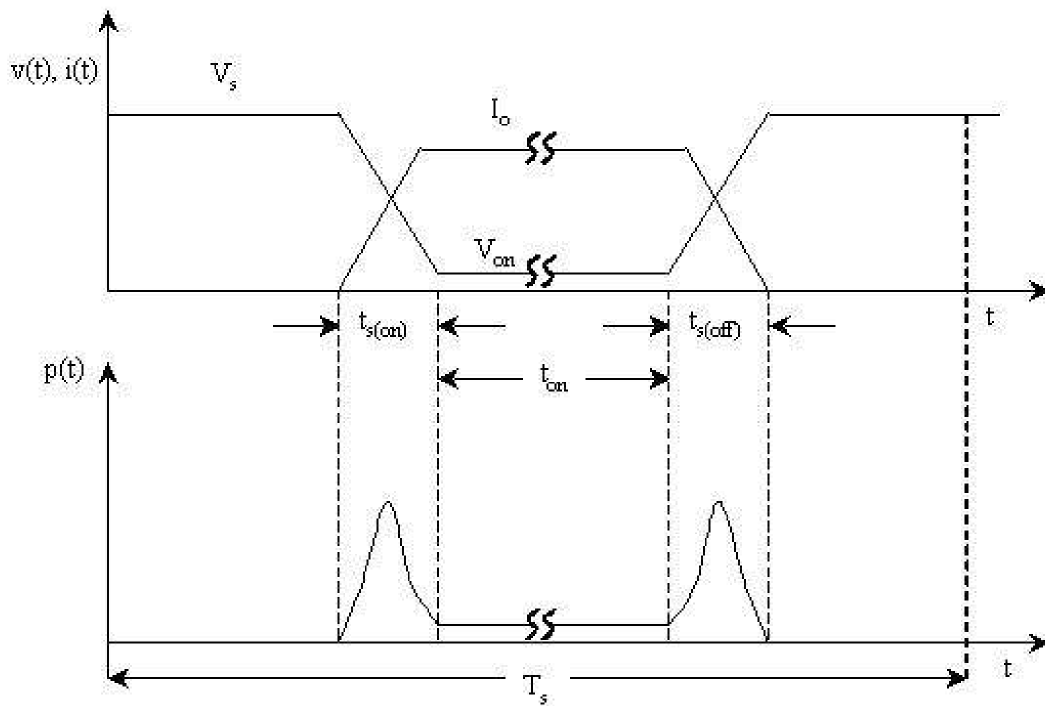

Figure 3.1. Controllable semiconductor switching characteristics

Total average power dissipation, $P_{t_{avg}}$, in semiconductors during one cycle of operation can be calculated by (3.1).

$$P_{t_{avg}} = \frac{1}{T_s}\int_0^{T_S} v(t)\cdot i(t)dt \tag{3.1}$$

where T_s denotes the period of one complete waveform, *v(t)* is the instantaneous voltage across the semiconductor, and *i(t)* is the instantaneous current through the semiconductor. The equation consists of power dissipated during the four states of operation. Equation 3.1 can be modified to calculate the average power for individual time periods to appear as (3.2).

$$P_{avg} = \frac{1}{T_s}\int_a^{b} v(t)\cdot i(t)dt \tag{3.2}$$

where *a* and *b* are the time boundaries for the semiconductor state of operation and T_s, *v(t)*, and *i(t)* are the same as (3.1). For example, the average power dissipated during conduction can be calculated between the interval *a* equal to t_2 and *b* equal to t_3 from Figure 3.1.

Although the instantaneous power during the turn-on and turn-off periods has the largest peak value, the time duration is small; therefore, using (3.2), the average power dissipated is small. Similarly, average power dissipated during block (blocking losses) are negligible because the leakage current is small. Thus, from (3.2), the average power dissipated during conduction can dominate the total average power because the time duration for this period is much larger than the turn-on or turn-off time periods and the forward current is much greater than in the blocking time period. However, the switching frequency plays an important role in the calculating the switching losses. The switching

frequency can reach a level where the power losses during switching dominate the total average power dissipated. This is a critical moment for the PE device because without a properly sized thermal management system, the heat energy is not dissipated quickly enough and the device will fail.

Because loss, during conduction, is the largest among a semiconductor's overall losses, Section 3.1.1 will use a piece-wise linear model method to determine the series resistance during the conduction time period. This method will be used to verify the experimental results, and give an accurate representation of the conduction losses associated with an increase in temperature.

3.1.1 Conduction Losses

A clear representation of the on-state, or conduction, characteristics of a minority carrier device (diode, BJT, or IGBT) can be determined by the *I-V* (forward current versus voltage) curve. From the *I-V* curve, the on-state voltage drop across the semiconductor is determined along with the series resistance. A typical diode *I-V* curve is shown in Figure 3.2(a), where the curve is modeled based upon (3.3).

$$I = I_s \left(e^{\frac{q(V - IR_S)}{nkT}} - 1 \right) \tag{3.3}$$

where I_s is the saturation current,

q is the magnitude of electron charge ($1.601 \text{x} 10^{-19}$C),

k is Boltzmann's constant ($1.3805 \text{x} 10^{-23}$ J/K),

T is the temperature in Kelvin,

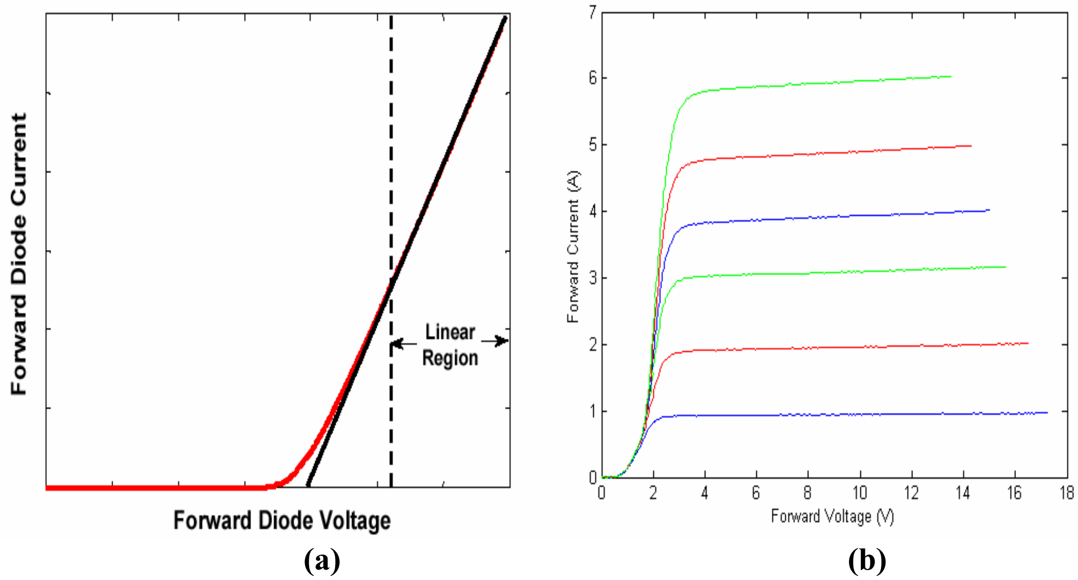

Figure 3.2. *I-V* characteristics (a) Typical diode (b) Tested IGBT

n is the ideality factor,

V is the voltage across the diode,

I is the current through the diode, and

R_s is the series resistance of the diode.

Power diodes, BJTs, and IGBTs operate in the linear region of the *I-V* curve shown in Figure 3.2(a). Figure 3.2(b) is a plot of the NPT-IGBT (Non-Punch-Through Insulated Gate Bipolar Transistor) semiconductor *I-V* curves that was tested with multiple forward currents. Clearly shown is the linear region, which can determine the series resistance and the on-state voltage drop across the device.

3.1.1.1 Piece-Wise Linear (PWL) Model

A piece-wise linear (PWL) model is an approximation of a diode, BJT, or IGBT parameters by representing the device during conduction as an ideal diode with all of its non-ideal characteristics modeled as a diode to prevent reverse current, a constant dc voltage drop, and a series resistor detailed previously in Figure 3.3(a). The parameters for the PWL model are taken directly from the *I-V* characteristics as shown in Figure 3.3(b) and (3.4). The x-intercept of the line is the PWL voltage drop, V_D, and the inverse slope of this line is the series conduction resistance, R_D, during the conduction period. V_F is the forward voltage across the device, and I_F is the forward current through the device.

$$V_F = \begin{cases} V_D & I_F = 0 \\ v_D + I_F \cdot R_D & I_F > 0 \end{cases} \tag{3.4}$$

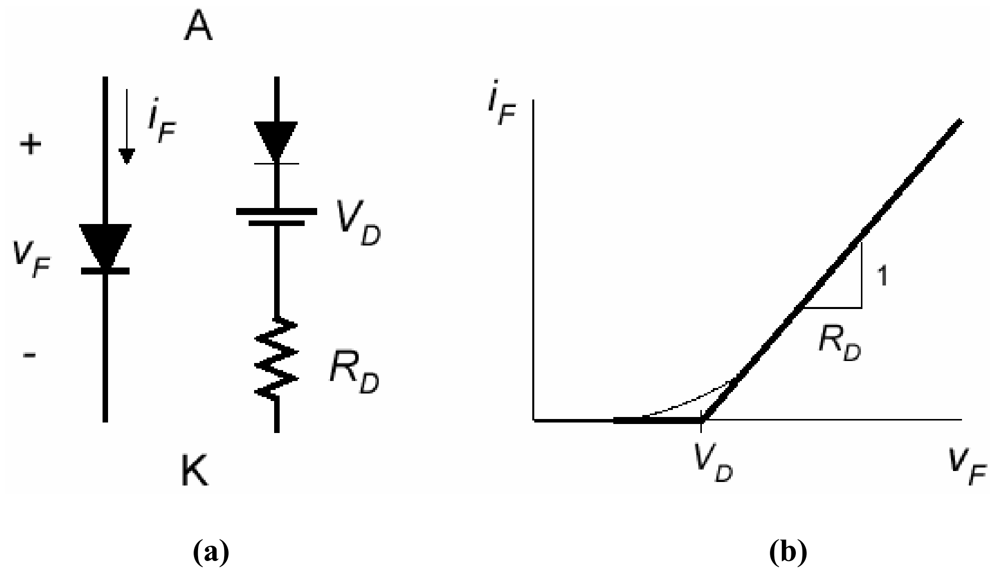

(a) **(b)**

Figure 3.3. PWL diode model **(a)** Diode symbol and PWL model **(b)** *I-V* curve of the PWL model

3.1.1.2 Calculating Conduction Losses

The voltage drop of the device, series resistance, and average and root-mean-squared values of forward current are the sources of a device's conduction losses. These losses can be expressed as:

$$P_{cond} = I_{avg} \cdot V_D + I_{rms}^2 \cdot R_D \tag{3.5}$$

where V_D and R_D are the PWL parameters found earlier and I_{avg} and I_{rms} are the forward current average and root-mean-squared values.

Equation 3.3 defines forward current as a function of temperature. The tested IGBT is a minority carrier device with a positive temperature coefficient meaning that as the temperature increases, so does the series resistance. As the series resistance increases so do conduction losses, which can cause catastrophic failure if the thermal energy is not managed within specification. Typically, the junction temperature of Si power devices is limited to 125 - 150°C, which is also directly proportional to device reliability. As rule of thumb, the failure rate for semiconductor devices doubles for each 10-15°C temperature rise above 50°C [1].

3.1.2 PWL Experimental Results

An experimental test was performed to study the effects of junction temperature on series resistance. The test procedure for determining the temperature characterization curves for the IGBT were as follows:

1. Modify a sacrificial IGBT by drilling a small hole into the junction layer and epoxy a type K thermocouple into the junction layer in an effort to accurately measure the junction temperature.
2. Place the sacrificial and tested IGBTs in a temperature chamber
3. Increase chamber temperature from 20ºC to 160ºC in 20°C increments.
4. Record the *I-V* curve data using a Characteristic Curve Analyzer and the tested IGBT at each target temperature.

The results of the experiment are shown in Table 3.1. Figure 3.4 is a plot of the experimental *I-V* curves. Observations made from the data taken include:

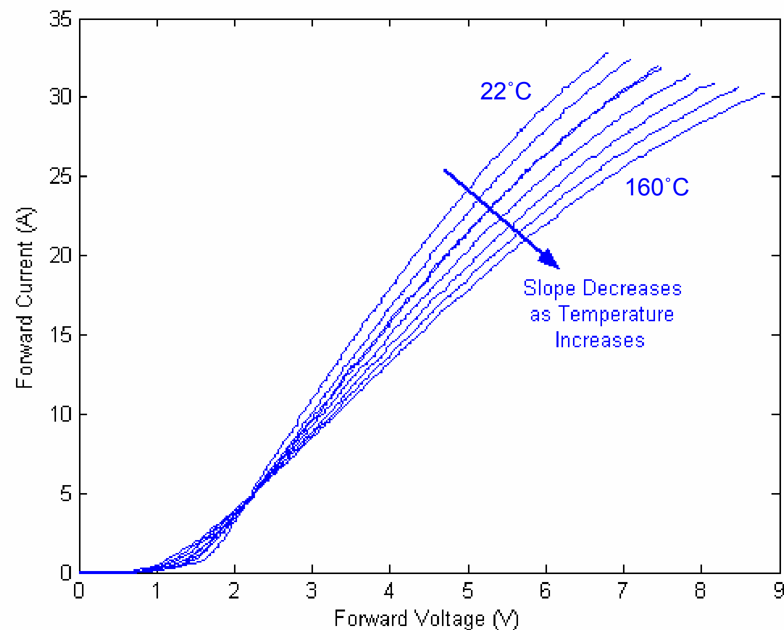

Figure 3.4. Temperature dependant *I-V* curves of the IGBT tested

Table 3.1. Temperature dependent R_D and V_D results of the IGBT tested

Temp (°C)	R_D (Ω)	V_D (V)	%diff R_D	%diff V_D	P_{cond} (W) at 6 A
22	0.0746	1.7067	0.00	0.00	12.9258
40	0.1103	1.5534	32.37	-9.87	13.2912
60	0.1586	1.3449	52.96	-26.90	13.779
80	0.1468	1.4026	49.18	-21.68	13.7004
100	0.1625	1.2964	54.09	-31.65	13.6284
120	0.1664	1.2497	55.17	-36.57	13.4886
140	0.1972	1.1289	62.17	-51.18	13.8726
160	0.1949	1.1139	61.72	-53.22	13.6998

1. The voltage drop across the device decreases and the series resistance increases as the junction temperature increases as shown in Figure 3.5.
2. The voltage drop decreases from 1.7067 V at 22ºC to 1.1139 V at 160ºC, a percent difference of 53%.
3. The series resistance increases 61.7% from 74.6 mΩ at 22ºC to 194.9 mΩ at 160ºC.

Suppose the forward current I_{rms} and I_{avg} are 6 A, using (3.5) and the values found in Table 3.1 for R_D and V_D, P_{cond} increases shown in Table 3.1. This confirms that maintaining a junction temperature at or close to 22ºC lowers the conduction losses and increases the efficiency and reliability of the PE device.

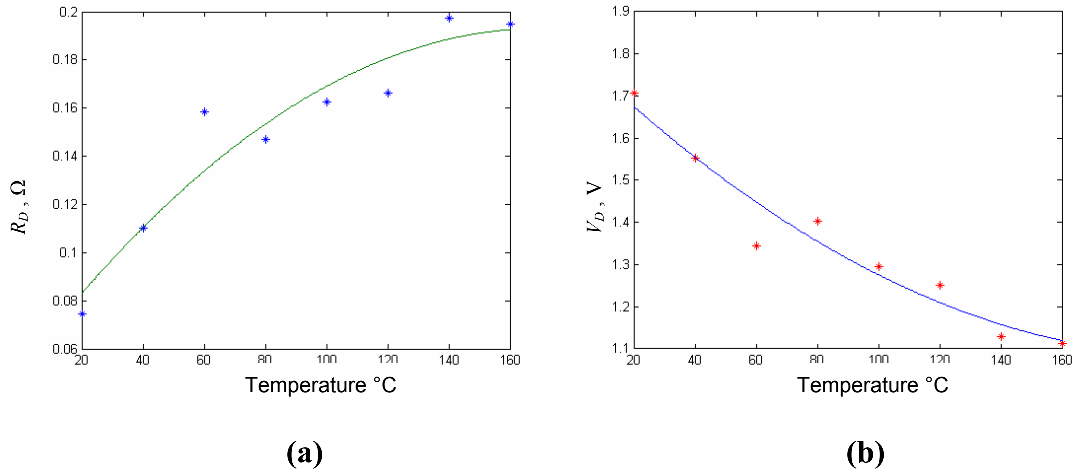

(a) **(b)**

Figure 3.5. PWL model parameters versus temperature **(a)** R_D vs. T **(b)** V_D vs. T

3.1.3 Switching Losses

Diode, BJT, and IGBT switching losses consist of the power dissipated during turn-on and turn-off time periods. Each of the three devices has minor differences during the switching process that contribute to differences in switching losses. Diode switching losses consist of turn-on, turn-off, and reverse recovery losses. The reverse recovery loss is dominant, while turn-on and turn-off losses are negligible. BJT and IGBT switching losses consist of turn-on and turn-off losses based on forward current and voltage. IGBT switching losses are usually smaller than BJT switching losses because of shorter switching times.

The switching losses for the experimental IGBT can be calculated using (3.2), where a and b are either t_1 and t_2 or t_3 and t_4 from Figure 3.1. The time period between t_1 and t_2 is the turn-on time $t_{s(on)}$. This is when the voltage across the semiconductor

transitions from the blocking voltage, V_s, to the conducting voltage, V_{on}. The converse is true for the turn-off time $t_{s(off)}$, the time period between t_3 and t_4. This is when the voltage across the semiconductor transitions from the conducting voltage, V_{on}, to the blocking voltage, V_s.

3.2 Experimental Results of Power Dissipation

This section will first present the experimental results of a comparison of the heat energy dissipated from an IGBT in an air cooled and R134a environments. Second, the test results from cooling the same IGBT by a mock automotive refrigerant system.

3.2.1 Air Cooled and R134a Cooled Experimental Results

In an effort to determine if R134a is a viable solution to cooling power electronics, a circuit was constructed and tested in both an air cooled environment and submerged in an R134a bath. The experimental circuit, a simple chopper circuit, consisted of a DC voltage source, IGBT, snubber circuitry, gate controller card, and a resistive load shown in Figure 3.6. (This experimental circuit resembles one sixth of a complete converter or inverter is used in HEV applications.) The experimental IGBT is a non-punch-through device with a rated continuous current of 13 A at 25ºC and maximum forward and blocking voltages of 600 V. A detailed specification list for the IGBT is included in Appendix I.

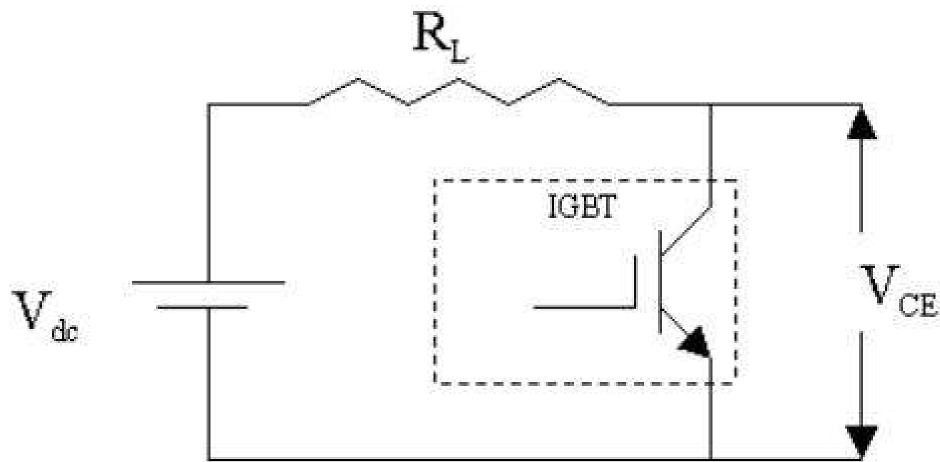

Figure 3.6. Experimental circuit

Both experiments were performed using the same circuit and components to insure no new variables other than cooling technique were introduced. The IGBT was cycled on and off at 1 kHz with a 50% duty cycle. The voltage V_{dc} applied was 480 V with a fixed load resistance R_L of 40 Ω that drew an average current of 6 A.

The R134a cooled circuit required a custom vessel to house the circuit and the R134a refrigerant. The vessel and setup is shown in Figure 3.7. The experimental vessel is comprised of a glass wall with an aluminum flange at the top and bottom enclosing the refrigerant. Interior to the vessel was the, IGBT, gate-controller card, and associated snubber components. The electrical connections for the DC-bus and gate-controller card are made via feed-through pins held in place using potted epoxy for a leak proof seal. No special coatings on the electronic equipment for electrical isolation or surface enhancement materials for increased heat transfer were used.

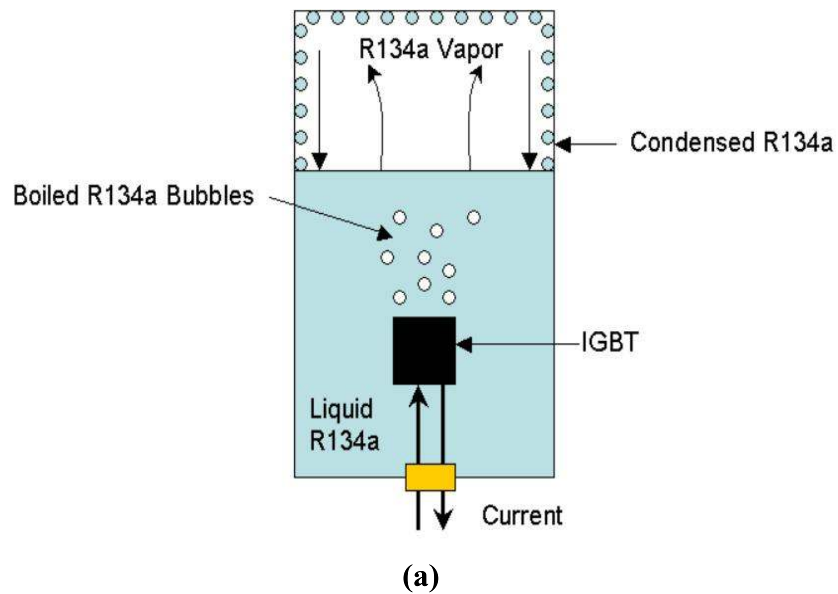

(a)

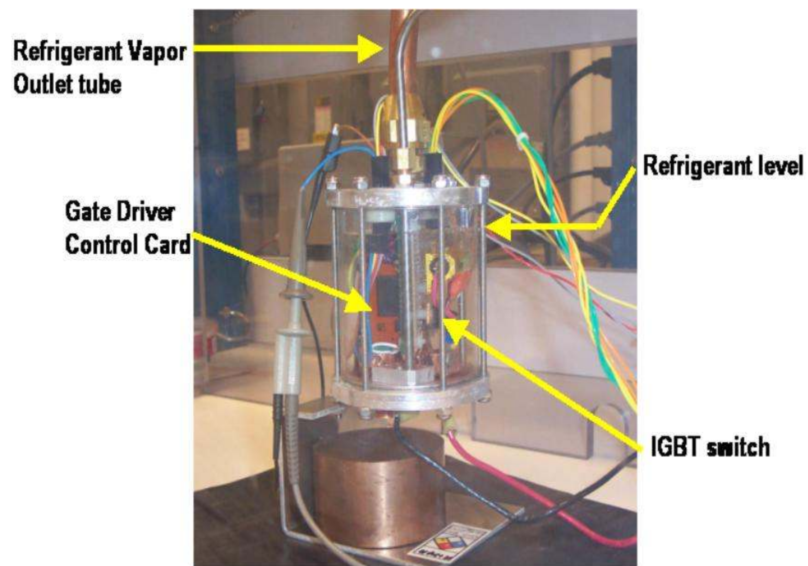

(b)

Figure 3.7. Experimental R134a system **(a)** Submerged IGBT cooling technique **(b)** Test vessel including PE circuit

As mentioned previously, the instantaneous voltage and current waveforms were obtained using a power analyzer. The power analyzer is an instrument that can digitally sample voltage and current, display their waveforms, store the waveform data, and perform associated power calculations. The test procedures for obtaining the instantaneous voltage and current waveforms for the air cooled circuit are as follows:

1. Configure power supply, V_{dc}, power analyzer, load resistors, R_L, and IGBT circuit as shown in Figure 3.8.
2. Activate gate controller card to cycle the IGBT at 1 kHz and 50% duty cycle.
3. Adjust the power supply to be in current control mode with a maximum average value of 6.0 A.
4. Use power analyzer to sample a complete period T_S.

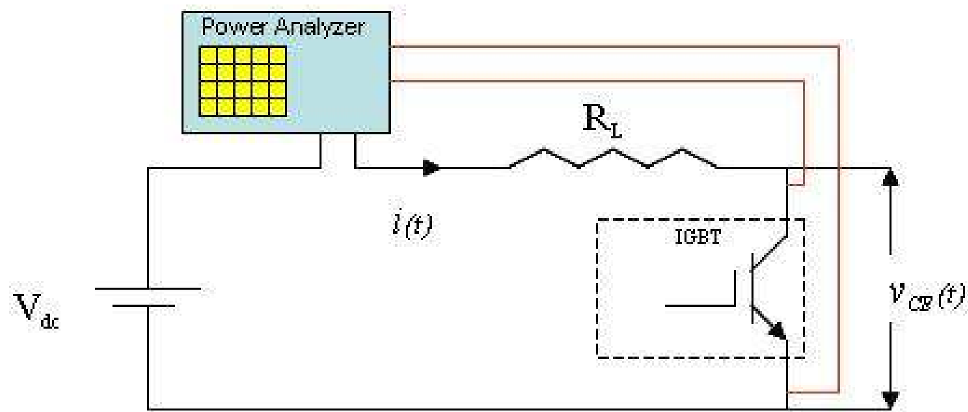

Figure 3.8. Experimental circuit containing power analyzer and connections

The test procedures for the R134a cooled circuit are the same as for the air cooled circuit with the exception of enclosing the circuit in the test vessel, pulling the interior of the test vessel into a vacuum, then filling the vessel with R134a to an appropriate level where the liquid is slightly above the circuit components.

The IGBT voltage and current waveforms are identical in both air-cooled and refrigerant-cooled environments. Figures 3.9(a) and (b) are views of voltage and current transitions for one complete period T_s. Figure 3.9(c) has an expanded view of the voltage turn-off and current turn-off transitions. Because the waveforms are identical it indicates that R134a does not change the IGBT turn-on and turn-off periods through the introduction of additional capacitance across the IGBT terminals or the gate-controller card. Additional capacitance could slow the IGBTs switching times by momentarily sustaining a voltage across the gate and source, V_{gs}, there by increasing switching losses. Figure 3.9(d) is a plot of instantaneous and average power for both tests. The average power loss for one complete period T_s of the refrigerant-cooled test was 24.73 W while the air-cooled test was 22.21 W.

The average power dissipated in Figure 3.9(d) was found using (3.1). Table 3.2 displays the results of average power dissipated from the IGBT in both the air cooled and R134a cooled environments. The average power for each switching instance of the switching cycle is found using (3.2).

Mentioned in section 3.1, average conduction losses are the largest power losses in semiconductors. This idea is shown in Table 3.2, where the average conduction losses for the experiments are the largest in magnitude among all switching periods. In the air

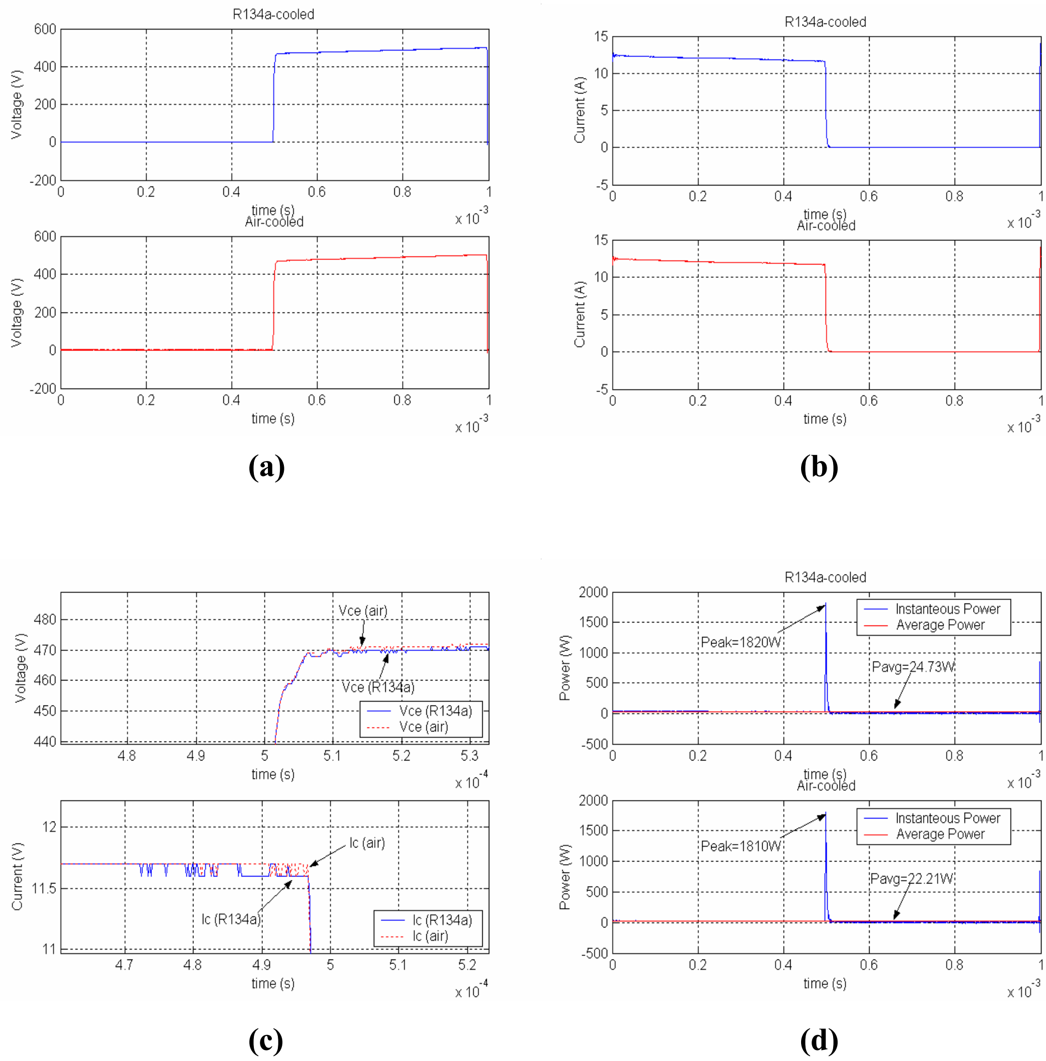

Figure 3.9. Experimental results for R134a-cooled and air-cooled power systems
(a) Voltage waveforms **(b)** Current waveforms
(c) Expanded voltage and current turn-off waveforms
(d) Instantaneous and average power loss

Table 3.2. Power dissipated from tested IGBT and PWL comparison.

	P_{total} (W)	$P_{blocking}$ (W)	$P_{s(on)}$ (W)	$P_{s(off)}$ (W)	P_{cond} (W)	P_{PWL} (W)	%diff P_{PWL} & P_{cond}
Air	22.12	2.65	0.38	5.85	13.24	13.88	4.8
R134a	24.73	2.26	0.41	5.75	16.32	15.70	3.8

cooled environment, the IGBT dissipates 13.24 W, while it dissipates 16.32 W in the R134a environment. The PWL model is compared to the experimental conduction losses. The PWL model calculates the conduction losses to be 13.88 W for the IGBT in the air cooled environment, and 15.70 W for the IGBT in the R134a cooled environment. These results are reasonably accurate as compared to the experimental results with only a small percent difference. Due to the marginal difference between the PWL model and experimental, it can be concluded that the PWL is an excellent means for determining the conduction parameters for semiconductors.

3.2.2 Automotive R134a Air Conditioner System Results

The results from the air cooled and R134a cooled experiments demonstrated that the refrigerant provides no interference with normal operation of the power circuit. These electrical components have been submerged in the refrigerant for over 300 days with no evidence of damage. Switching characteristics of the IGBT were not affected; therefore, to take full advantage of the thermal characteristics of R134a, the circuit is operated simultaneously with the mock automotive A/C system shown in Figure 3.10.

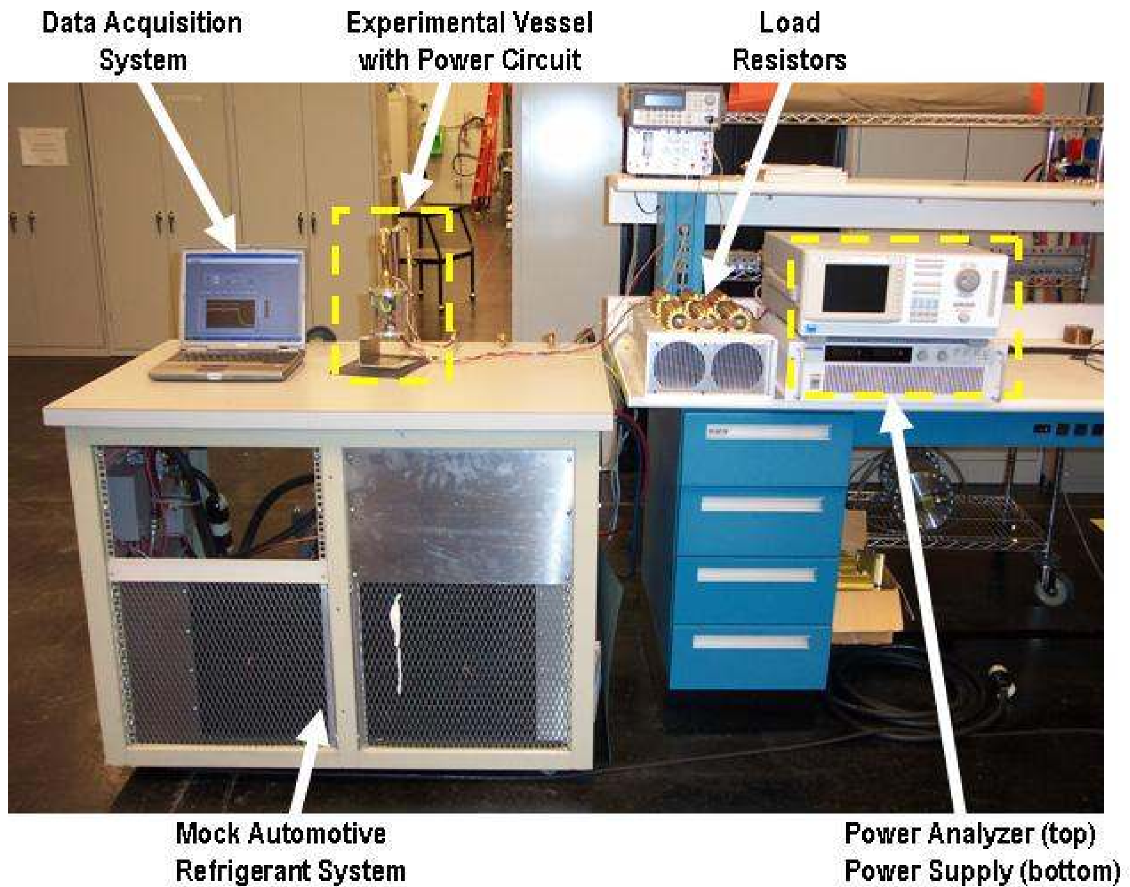

Figure 3.10. Mock automotive air conditioner system with vessel and power circuit

The mock automotive A/C system is constructed from components that comprise a 2003 Buick Park Avenue A/C system, which includes a compressor, condenser, evaporator, and control system. A 5 hp, three-phase induction motor provides the compressor with mechanical power. Two service ports are placed in parallel with the evaporator refrigeration circuit to provide external mounting and operation to the test vessel. The automotive A/C system has 9320 W of cooling capacity for cooling the cabin, which should provide plenty of capacity for cooling the IGBT and proven later.

The objective of this experiment is to observe the IGBT case temperature, IGBT voltage and current waveforms, and air conditioner system behaviors during simultaneous operation. The procedures were as follows:

1. Enclose experimental IGBT circuit in the test vessel, and connect associated refrigerant lines to the air conditioner system.
2. Pull a vacuum in the vessel and refrigerant lines.
3. Fill vessel and refrigerant lines to appropriate level.
4. Follow 1 through 4 of air cooled circuit procedure.
5. Activate air conditioner system and open service valves to cycle refrigerant through the vessel.
6. Monitor the refrigerant liquid level and make necessary adjustments.
7. Turn-on power supply and power analyzer and monitor instantaneous voltage and current waveforms.
8. Increase current by 1 A in 30 minute intervals from 6 A to 10 A.

The test required temperature acquisition devices to capture, analyze, and record ambient, IGBT case, and vessel refrigerant temperatures. A LabView program was

written to analyze and record temperature data from Model # 44008 thermistors. More detail of the LabView program is given in Appendix III. One thermistor was attached to the body of the IGBT using epoxy to capture the IGBT case temperature. It was placed in the IGBT's screw hole, which would not interfere with the operation of the IGBT or the refrigerant's ability to remove heat energy from the IGBT. Another thermistor was submerged in the R134a liquid to capture the vessel temperature. Analyzing the temperatures will quantify how much the mock automobile A/C system will cool with the PE devices.

The test results from the mock A/C test are shown in Figures 3.11 and 3.12. Figure 3.11 is a plot of the ambient, IGBT case, and vessel refrigerant temperatures versus time. The IGBT case temperature was calculated to be 4.2°C, while vessel refrigerant was on average 1.1°C and the ambient temperature was 22.9°C outside the test vessel. The ambient, IGBT case, and vessel refrigerant temperatures remain nearly constant throughout the average forward current levels of 6, 7, 8, and 9 A. A failure to the IGBT occurred at the beginning of the 10 A test. Evidence indicated that the IGBT was conducting a peak current of 20 A for approximately 0.5 ms, which is beyond the rating of the device.

The IGBT experienced a failure during the first moments of the 10 A test. The failure was determined to have been caused by three factors:

1. Operating the IGBT near rated voltage.
2. Conducting 20 A for half of period (0.0005 s).
3. Large stray inductance in the circuit that produces significant voltage and current overshoots during turn-off.

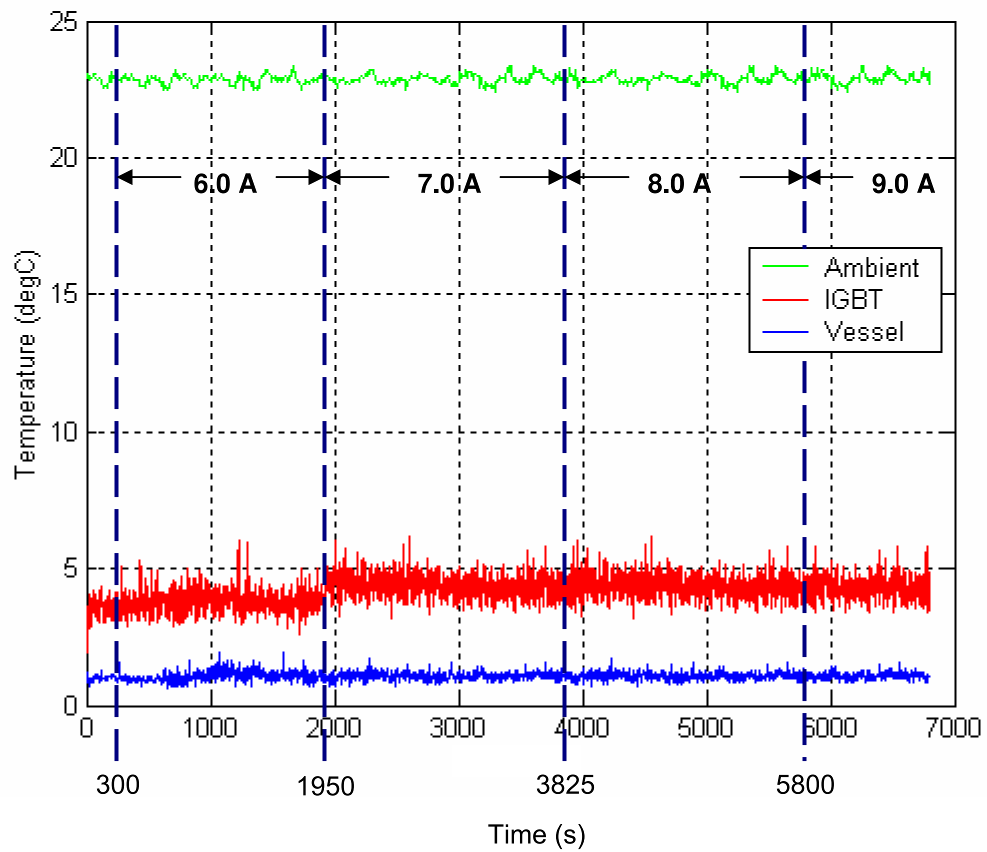

Figure 3.11. Temperature versus time from refrigeration test

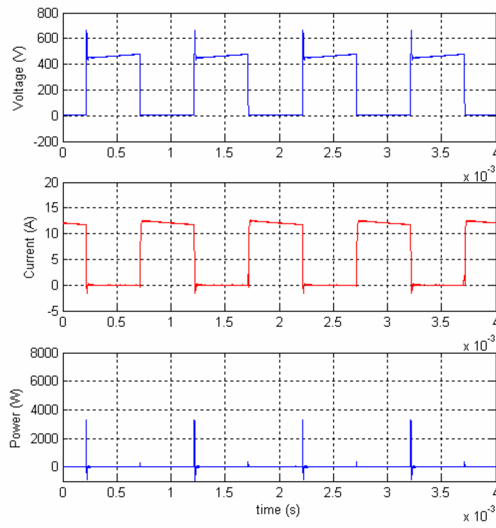

(a)

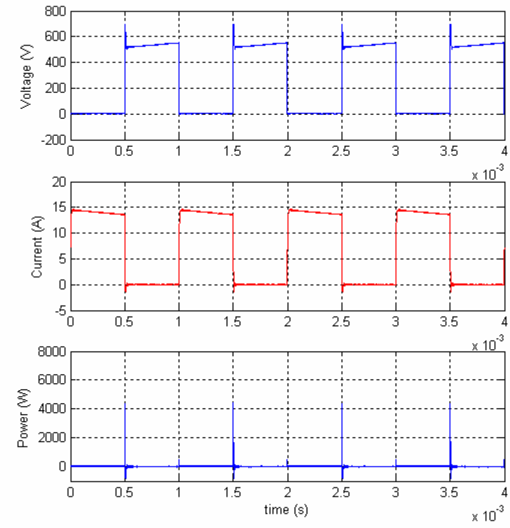

(b)

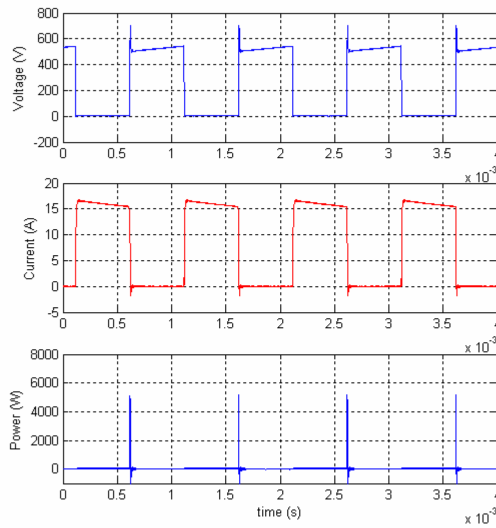

(c)

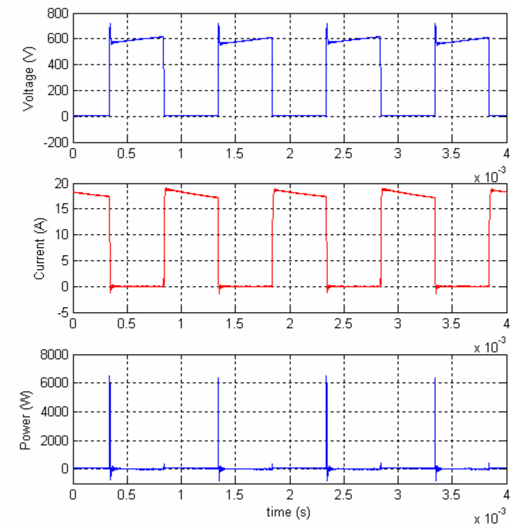

(d)

Figure 3.12. Instantaneous voltage, current, and power waveforms from automotive air conditioner system cooling IGBT
(a) 6 A test **(b)** 7 A test **(c)** 8 A test **(d)** 9 A test

Figure 3.12(a)-(d) are plots of the instantaneous IGBT voltage $v_{ce}(t)$, current $i_c(t)$, and power $p(t)$ for the average current levels of 6, 7, 8, and 9 A. From Figure 3.12, the refrigerant system does not disturb the normal operation of the IGBT voltage and current.

The efficiency of the IGBT is an indicator of performance in PEs. Efficiency is determined by comparing the total average power dissipated from the complete system and the average power dissipated by the PE device. The efficiency, η, is calculated using (3.6). The IGBT efficiency during the preceding test is calculated to be 99%, which is illustrated in Table 3.3.

$$\eta = \frac{P_{out}}{P_{in}} \cdot 100\% = \frac{V_{dc} \cdot I_{avg} - P_{IGBT}}{V_{dc} \cdot I_{avg}} \cdot 100\% \qquad (3.6)$$

Conclusions from the data in this test indicate a typical automotive A/C system has more than sufficient cooling capacity to cool the single test IGBT. As the temperature of the IGBT case remained well below ambient temperature, it can be concluded that the A/C system can dissipate more heat from additional PE devices.

Table 3.3. Efficiency of IGBT

I_{avg} (A)	V_{dc} (V)	P_{total} (W)	P_{IGBT} (W)	%eff η
6.00	461	2766	25.5	99.1
7.00	533	3731	34.2	99.0
8.00	522	4176	39.7	99.0
9.00	587	5283	54.7	98.9

3.3 Summary

Silicon (Si) based power electronics devices are based on four states of operation, which includes conduction, blocking, turn-on, and turn-off. The instantaneous power dissipated during each state can be calculated using $v(t) \cdot i(t)$, where *v(t)* is the voltage drop across the device and *i(t)* is the forward current through the device. A power circuit containing an IGBT, gate controller card, and snubber was built to study the power dissipation device and switching characteristics in a PE. An open air and a submerged test were performed on the circuit to study the switching characteristics of the circuit in the R134a bath, and the results indicate that the refrigerant offers no alterations to the circuit. A piece-wise linear (PWL) model was developed using the forward characteristics of the IGBT, then compared to the average conduction losses found by $v(t) \cdot i(t)$. The percent difference for the PWL model was within 5%. And then the circuit was tested while being cooled by a mock automotive air conditioning system. Conclusions from the data in this test indicate a typical automotive air conditioner system has more than sufficient cooling capacity to cool the single test IGBT. As the temperature of the IGBT case remained well below ambient temperature, it can be concluded that the air conditioner system can dissipate more heat from additional PE devices.

Chapter 4

SYSTEMS AND SIMULATION

In the previous chapter, an IGBT circuit was the subject of a series of tests that provided evidence showing that R134a has good dielectric properties for the voltage and current range found in HEVs, in addition to having excellent cooling effects on a single IGBT. This chapter will take the results of chapter 3 and extrapolate the results to a three-phase, six-IGBT inverter similar to what is found in HEV applications. The requirements for the inverter are taken directly from the FreedomCAR specifications, and it will be simulated using custom thin-film resistors in the mock automotive A/C system.

4.1 Three-Phase Inverter

From chapter 1, an HEV is propelled via an IC engine and an electric motor. Electric motors are manufactured in many voltage and horsepower ratings. While many HEV configurations are possible (series, parallel, hybrid, etc), the common denominator to all of them is the usage of PEs for the interface and control of the electric motor. The electric motor of HEVs is typically a three-phase motor because of their convenience in non-traction applications. The PE package used to control the electric motor is called the 'inverter', which is designed to shape and control the three-phase output voltages in magnitude and frequency. Using an inverter, HEVs can change the on-board battery's dc voltage to a three-phase sinusoidal voltage suitable for traction drive motors. A three-phase inverter consists of three switching legs, one leg per phase, as shown in Figure 4.1.

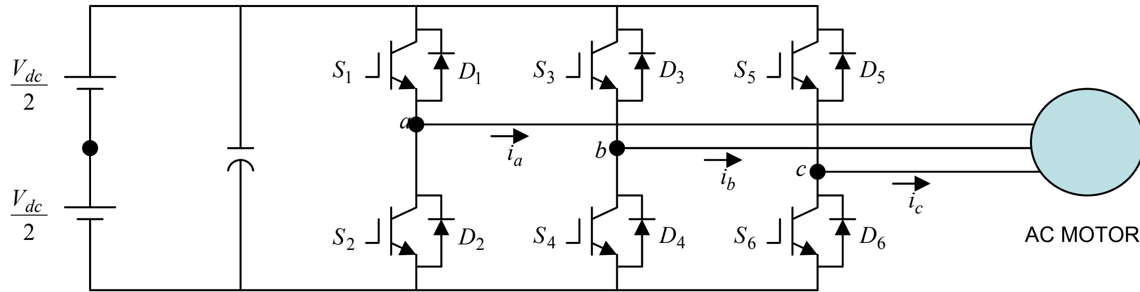

Figure 4.1. Three-phase inverter driving an ac machine

Each switching leg contains two PE switching devices in series for a total of six switches within the inverter.

The most common switching method uses a unipolar switching method for a pulse-width- modulated (PWM) output voltage waveform. Unipolar switching method uses a sinusoidal control waveform at the same frequency as the desired output fundamental frequency. This control waveform is then compared to a carrier triangular waveform, which determines the firing pattern for the switch. In a three-phase inverter, each leg has a control waveform 120° out of phase with each other, and all three waveforms are compared to one carrier wave, illustrated in Figure 4.2(a). The output line-to-neutral voltage waveform for leg a, V_{an}, is shown in Figure 4.2(b). Likewise, the

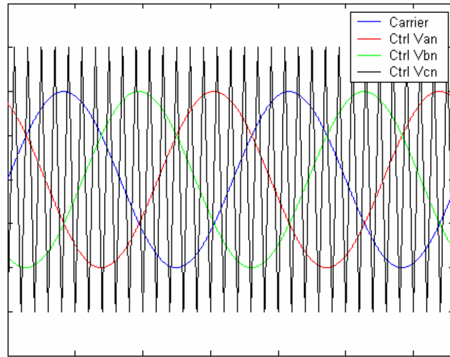

(a)

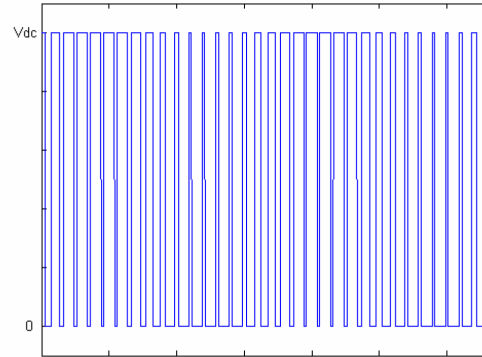

(b)

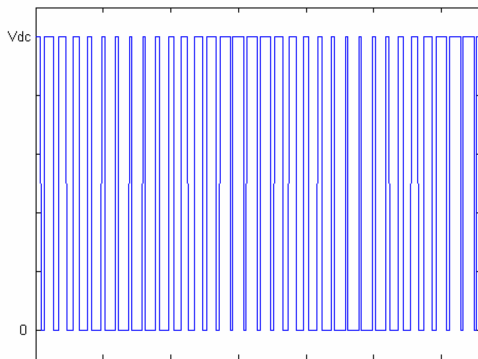

(c)

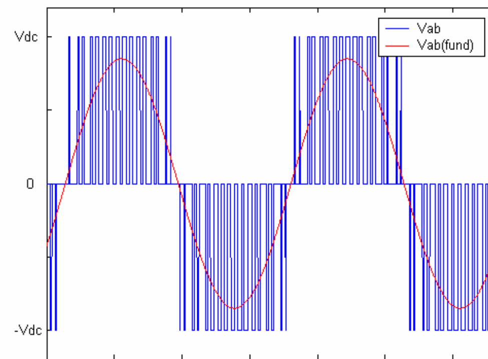

(d)

Figure 4.2. Characteristic waveforms for three-phase inverter
(a) Carrier triangle wave and control waveforms
(b) V_{an} output waveform
(c) V_{bn} output waveform
(d) V_{ab} output waveform

output voltage waveform for leg b, V_{bn}, is shown in Figure 4.2(c). The output line-to-line voltage waveform is found by (4.1) and shown in Figure 4.2(d).

$$V_{ab}(t) = V_{an}(t) - V_{bn}(t) \tag{4.1}$$

Mentioned in Chapter 1, the FreedomCAR partners developed a list of design requirements to be used in the next generation of HEV vehicles. One requirement of the FreedomCAR is that the electric propulsion system, including inverter, must be capable of delivering 30 kW of continuous power. The efficiency of the inverter is an important factor among HEV engineers because it is an indicator of wasted power converted into heat by the PE devices. The wasted power robs the power from the motor and draws extra power from the batteries. Efficiency for an inverter is based on many variables such as semiconductor ratings, switching frequency, supply voltage, phase current, stray inductance, etc. Typically, an inverter's efficiency is 96%; therefore, an estimated loss for a 30 kW inverter is 1200 W continuous.

In the next section, the inverter will be simulated using six thin-film resistors as the PE devices. Resistors are used because the power loss in an inverter is considered purely resistive, and an I^2R loss can model the continuous power loss of each IGBT during switching. The resistors are cooled by the mock automotive A/C system to emulate heat from an inverter.

4.2 Thin-Film Resistor

An industry leader in the manufacture of thin-film components, Vishay Electro-thin-film Films, produced a custom thin-film resistor for the Oak Ridge National

Laboratory designed to resemble the footprint of a small PE device. The physical dimensions of a resistor are 0.51 cm by 0.83 cm by 0.05 cm, and it has a value of 10 Ω. The manufacturers did not provide any specifications of the resistors; therefore, power dissipation, current, and temperature limits were unknown.

Our main objective is to test the resistors in a method that best simulates the power dissipation of an inverter used in an HEV application during normal operation. From section 4.1, the average power dissipated by the PE devices in the form of waste heat was estimated to be 1200 W.

Six resistors were configured into a circuit as shown in Figure 4.3. Three parallel branches of two parallel resistors were placed into the vessel, used and described previously, and connected to an external dc power supply. The experimental procedures used to test the power dissipation capabilities of the system were the following:

1. Enclose the resistor circuit in the test vessel, and connect associated refrigerant lines to the air conditioner system.
2. Pull a vacuum in the vessel and refrigerant lines.
3. Fill vessel and refrigerant lines to appropriate level with refrigerant.
4. Activate air conditioner system and open service valves to cycle refrigerant through the vessel.
5. Monitor the refrigerant liquid level and make necessary adjustments
6. Turn-on power supply and monitor voltage and current meters.
7. Record the temperatures of each resistor branch and vessel refrigerant.
8. Increase current by 1 A intervals beginning at 16 A after resistor temperatures reach steady state

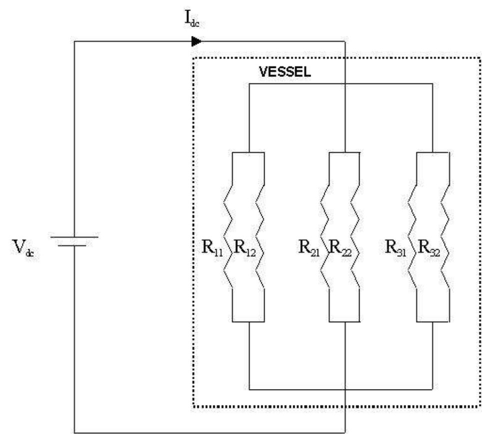

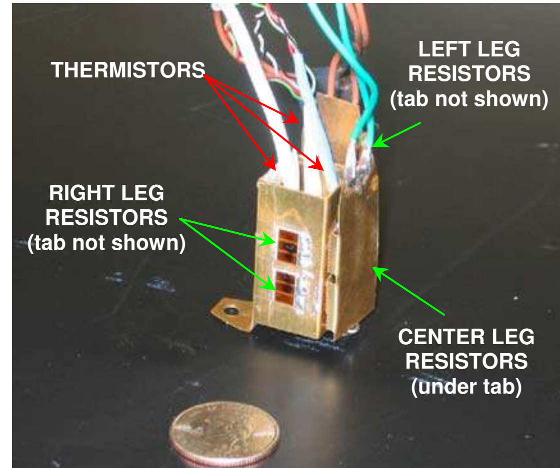

(a) **(b)**

Figure 4.3. Thin-film resistor circuit **(a)** Circuit diagram **(b)** Resistor assembly

Each branch temperature represents the case temperature of the IGBT device in that branch. A plot of the resistor temperatures of each branch versus time is shown in Figure 4.4. At a first look, the resistor temperatures are different because of the configuration of the resistors; see Figure 4.3(b). The center resistor branch receives heat energy from the two neighboring resistor branches conducted by the metal substrate to which the resistors are mounted, which increases the center branch resistor temperature. The left branch is the coolest because it is placed closest to the inlet refrigerant tube, where a fresh supply of refrigerant is being forced across the branch.

Initially the resistors dissipate 422 W at 16 A as illustrated in Table 4.1, which shows each interval of power dissipation. During this period, temperature fluctuations are present due to adjustments on the bulk refrigerant level within the vessel. Once the liquid level settled, the current was increased to 18 A, and the total power dissipated was

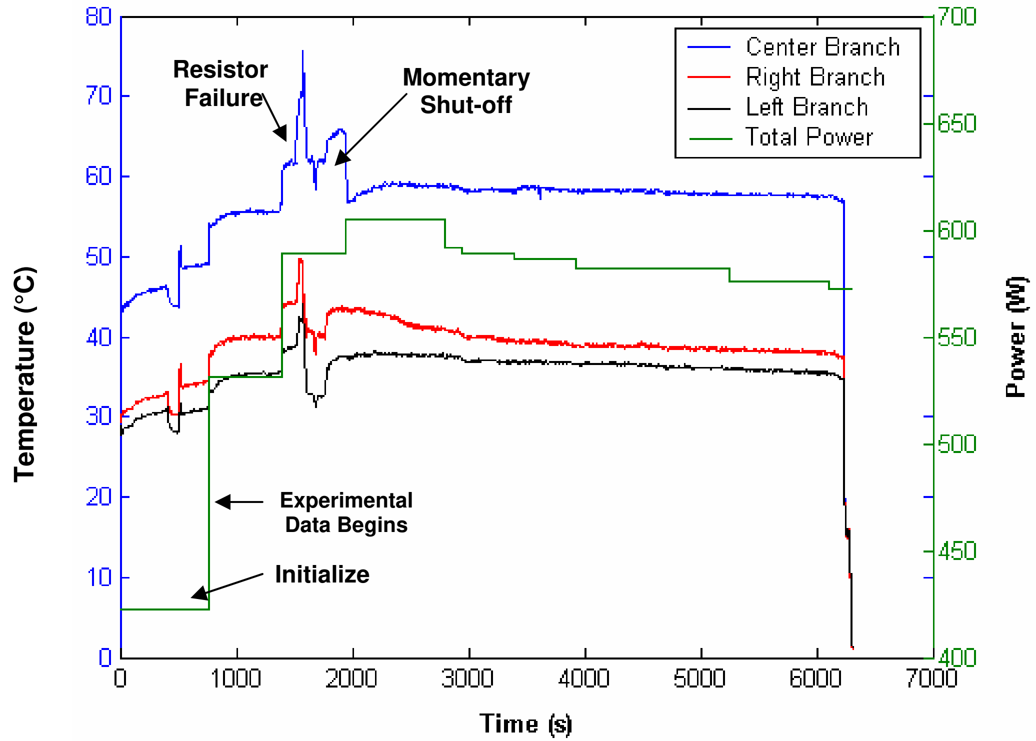

Figure 4.4. Resistor temperature and power dissipation versus time

Table 4.1. Thin-film resistor experimental results

		Branch Temperature (°C)		
I_{avg} **(A)**	P_{total} **(W)**	**Center**	**Right**	**Left**
16.0	422	55.5	39.7	35.4
18.0	531	56.6	40.9	36.0
19.0	589	61.8	43.9	38.5
18.4	605	58.9	41.0	37.7
18.0	592	58.8	40.8	37.5
17.9	589	58.3	38.7	36.9
17.8	586	58.3	39.2	36.8
17.7	582	58.1	38.7	36.5
17.5	576	57.5	37.8	35.5
17.4	572	57.5	37.7	35.4

531 W. The center, right, and left branch temperatures reached a steady state temperature of 55.5°C, 39.7°C, and 35.4°C respectively. The current level was then set to 19 A, and the total power dissipated was 589 W. After 100 seconds, a portion of the center branch resistor failed at a temperature of 61.8°C. The center, right, and left branch temperatures reached a peak of 75.6°C, 49.7°C, and 44.0°C respectively; at which point, the power supply was deactivated for 80 seconds. A decision was made to continue the experiment and the power supply was again activated.

Because of the failure, the center branch resistance was altered from 5 Ω to 6.3 Ω; therefore, more power would be dissipated from the center branch resistors. A decrease of current from 19.0 A to 18.4 A was set, which resulted in a new power dissipation of 605 W. During this period, the center, right, and left branch temperatures leveled to 59.2°C, 41.5°C, and 37.7°C respectively. Once again, the center resistor begins to fail, but the power supply was set at a voltage and current limit to prevent a complete failure. From Figure 4.4, the power dissipated takes a series of decreasing steps because of more resistor failures until ultimately deactivating the power supply terminated the experiment.

The results of the experiment demonstrate that the automotive air conditioner is capable of cooling the resistors up to 605 W. The power ratings of the resistors was unknown, although a reasonable conclusion based upon the experimental results is that if the resistors have a larger current rating, the automotive A/C could sustain the resistor temperatures below 120°C at power levels beyond 600 W.

In the next section, the data is extrapolated to determine the temperatures of each branch resistors and bulk refrigerant temperature while dissipating 1200 W.

4.2.1 Thin-Film Resistor Extrapolation

The thin-film resistor experiment presented insightful data as to the effectiveness on PEs and cooling capacity of the mock A/C system. From this experiment, the data is used to model the temperatures of each branch of resistors and bulk refrigerant temperature while dissipating 1200 W. The branch temperature will represent the case temperatures of each IGBT device in that branch.

A temperature curve versus average forward current is extrapolated for each branch of resistors and bulk refrigerant temperature as shown in Figure 4.5. The results from the plots are shown in Table 4.2, where the inverter dissipating 1200 W of loss, the center, right, left, and bulk temperatures are 107˚C, 75.5˚C, 60.0˚C, and 40.8˚C respectively. Finite analysis would be needed to determine the junction temperatures of each IGBT because the heat distribution is non-uniform among the resistor arrangement.

Table 4.2. Extrapolated thin-film resistor results

		Branch Temperature (°C)			
I_{avg} (A)	**P_{total} (W)**	**Center**	**Right**	**Left**	**Bulk**
0.0	0	0.0	0.0	0.0	0.0
10.0	165	17.8	13.1	14.5	10.0
20.0	659	61.5	43.9	38.4	26.3
27.0	1201	107.1	75.5	60.0	40.8
30.0	1483	130.5	91.6	70.5	47.9
34.0	1905	165.2	115.6	85.6	58.0

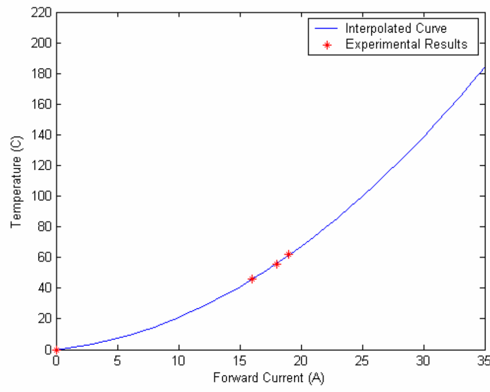

(a)

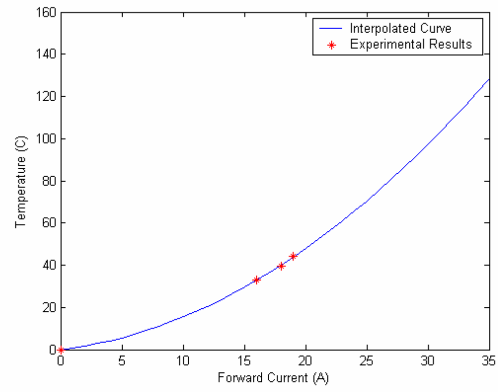

(b)

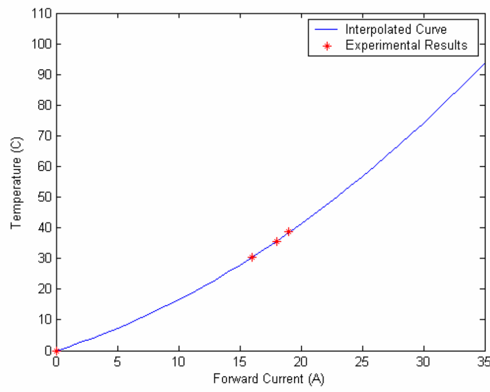

(c)

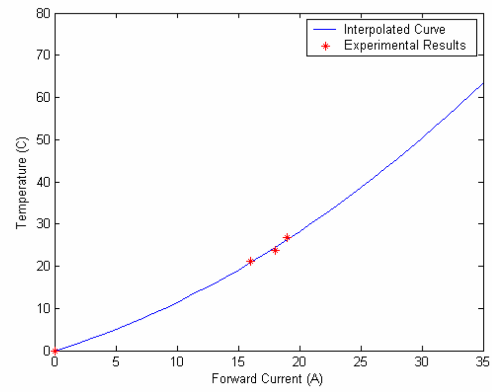

(d)

Figure 4.5. Extrapolated temperature versus average forward current curves **(a)** Center branch **(b)** Right branch **(c)** Left branch **(d)** Bulk refrigerant

An inverter loss of 1200 W is in agreement with the maximum cooling capacity of 9320 W specified for the automotive air conditioner based upon communications with General Motors, the air conditioner manufacturer [15]. This cooling capacity of 9320 W is well above the 1200 W needed to cool the mock inverter and is viewed as a baseline for typical A/C cooling capabilities.

4.3 Active IGBT Junction Cooling Simulation

Experimental results from sections 3.2.2 and 4.2 demonstrate that the removal of heat energy from the generating area is the limiting factor for large forward current capabilities in PE devices. Using the IGBT in chapter 3 as an example, the junction to case thermal resistance is 2.1 Ω, which translates into a significant difference in temperature between the case and the junction. Presented in this section is theoretically removing the case from the junction, and simulating actively cooling the IGBT junction layer.

The case is a special polymer-resin based plastic to physically shield the IGBT junction from impact and contaminates damage. The case is engineered to be thermally conductive; however, the metallic backing plate performs the majority of the heat transfer. However, the backing plate is unable to provide enough heat dissipation at large current levels, and an example of which is shown in section 3.2.2 where the IGBT failed at 10 A of forward current but the case temperature was 5˚C. The case is physically unable to be removed from the actual Si below, as the case is a cast-in-place design with the gate, collector, and emitter pins embedded in the plastic. Theoretically separating the

case from the junction will be explored where the junction layer will be exposed to the ambient. Also, the gate, collector, and emitter pins shall be accessible, and a possible special coating applied only to shield the Si from contaminates. The special coating is estimated to be a few millionths of an inch applied to the surfaces of the junction layer, and it shall have a thermal resistance of 0.5 Ω, similar to thermal grease, which is applied between a PE device and a heat sink to provide even thermal conductivity. The thermal resistance value was taken from the data sheet for the IGBT found in Appendix I.

4.3.1 Single IGBT Simulation

The junction layer temperature T_j of a single exposed junction IGBT is simulated and compared to a cased IGBT. The IGBTs are operating under the same switching frequency, duty cycle, and refrigerant temperature to minimize error. The simulation incorporates the steady state thermal circuit model of the IGBT and cooling system described earlier in chapter 2.

The thermal circuit model is shown in Figure 2.1. Equation 2.3 describes the junction temperature as a function of the thermal resistance between the junction and ambient, ambient temperature, and average power dissipated by the IGBT. From the results of the IGBT experiment in section 3.2.2, Figure 4.6 displays the average power dissipated for the average forward currents of 6, 7, 8, and 9 A. Using quadratic approximation, the average power dissipated follows (4.2).

$$P = a_1 i_{avg}^2 + a_2 i_{avg} + a_3 \qquad (4.2)$$

where: P = Average power dissipated,

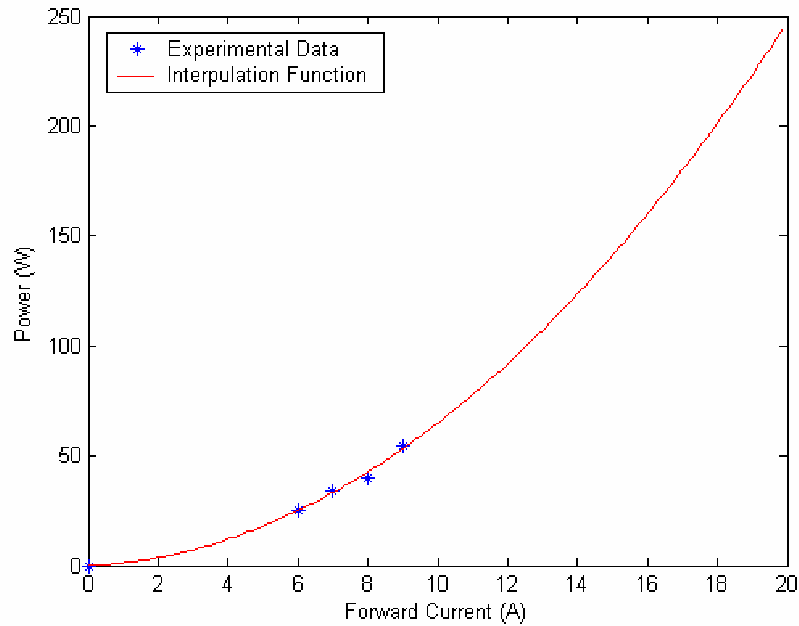

Figure 4.6. Average power dissipated versus forward current

i_{avg} = Average forward current,

$a_1 = 0.58545$,

$a_2 = 0.63624$,

$a_3 = 0.071967$.

Thermal resistance for junction to case, R_{j-c}, and junction to thin-coating, R_{j-co}, were determined in section 4.3. The case to R134a, R_{c-r}, was determined from results in section 3.2.2 and thermal circuit analysis. The temperature of the IGBT case, T_c, is equal to 3.0°C, temperature of the refrigerant, T_r, is equal to 1.5°C, and the total average power dissipated by the IGBT is equal to 25.5 W, therefore, $R_{c-r} = \dfrac{T_c - T_r}{P_{total}} = 0.0588\,\Omega$. The thermal models to be simulated are shown in Figure 4.7.

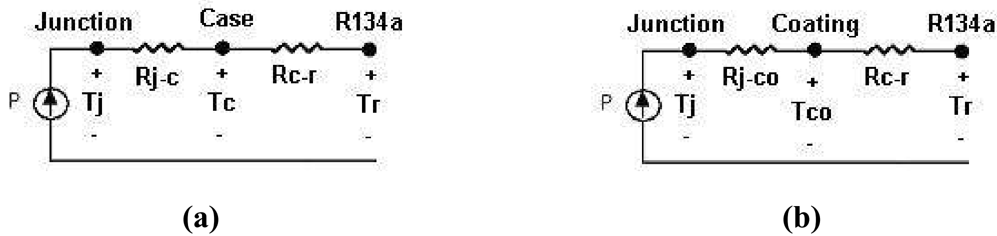

Figure 4.7. Thermal model **(a)** IGBT with case **(b)** IGBT with exposed junction

The simulation will hold constant the switching frequency and duty cycle while varying the total average power dissipated and forward current. The simulation results are shown in Figure 4.8, which show that as forward current increases, the junction temperature increases for both IGBTs. The manufacturer determined the maximum temperature to be 125°C. The IGBT with the attached case experiences a maximum junction temperature at 8.5 A; however, the exposed junction IGBT reaches 17.5 A before meeting the maximum junction temperature. At 17.5 A, the junction temperature of the IGBT with a case was estimated to be 423°C by simulation.

HEVs would be an ideal application for an inverter built from exposed junction IGBTs because the inverter would be smaller, lighter, and more reliable than present designs. Smaller, lighter inverters because the IGBTs they will not have a bulky case. The IGBTs have a greater current capability; therefore, they will not have to be overrated.

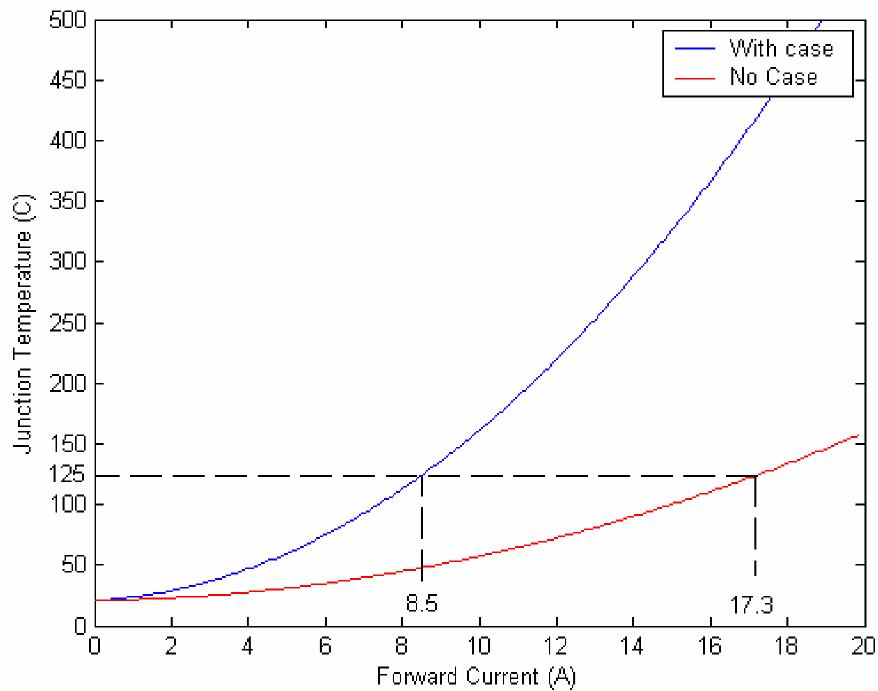

Figure 4.8. Junction temperature versus forward current

4.4 Summary

In this chapter, PEs were shown to be used in an inverter to control the electric motor in an HEV. These PE devices have losses in the form of heat energy associated with switch operation. The average power dissipated by an inverter was estimated to be 1200 W. To experimentally model the inverter, six thin-film resistors were used to study the cooling effects on PEs and capacity of the automotive A/C system. The results of the experiment demonstrate that the A/C system is capable of cooling the resistors up to 605 W, where the thin-film resistors began to fail due to the high current. However, the experimental data was extrapolated to determine the branch resistor and bulk refrigerant temperatures at 1200 W. And then, an active IGBT junction cooling technique was introduced, where the case is removed, and the junction is directly cooled by the R134a

refrigerant. The simulation results show that an IGBT with the attached case experiences a maximum temperature of 125˚C at 8.5 A; however, the exposed junction IGBT reaches 17.5 A before meeting the maximum junction temperature. This technique maximizes the effectiveness of the R134a cooling system and the forward current capability of the PE device.

Chapter 5

CONCLUSION AND FUTURE WORK

5.1 Conclusion

Summarizing the contributions of this research endeavor, the chief motivation of this work was based on finding an alternative to conventional power electronics cooling methods for hybrid-electric vehicle applications. PEs are vital to the operation and performance of HEVs because they provide the interface between the energy sources and the traction drive motor. As with any "real" system, PE devices have losses in the form of heat energy during normal switching operation, which has the ability to damage or destroy the device. Thus, to maintain reliability of the PE system, the heat energy produced must be removed. Present HEV cooling methods provide adequate cooling effects, but lack sufficient junction temperature control to maintain long-term reliability.

The technique described in this thesis incorporates R134a refrigerant and the on board air conditioning system to keep PE devices in a reliable range of temperatures. Proven by experimentation, R134a has no damaging effects on the normal operation for 300 days on a submerged IGBT, gate controller card, and snubber circuits. The IGBT circuit was operated in an air cooled and R134a environment where the voltage and current waveforms were compared. Results indicate R134a induces no additional delay or switching losses for the IGBT circuit. The automotive air conditioner system provided a constant case temperature of 4.2°C.

The automotive air conditioner system was shown to have more than adequate cooling capacity to cool a six-IGBT inverter. Based on FreedomCAR specifications, normal operation of the inverter IGBTs will dissipate 600 W of heat energy. The thin-film resistor experiment proved that the automotive air conditioning could keep the junction temperature well below the 125°C target.

In addition, experimental data discussed in this thesis proved that the thermal resistance of the case limits a PE device's ability to remove heat energy from the junction layer. A simulated comparson of an IGBT with a case attached and an exposed junction IGBT was performed using experimental results. The results from the simulation indicate the exposed junction IGBT technique would benefit by reducing the junction temperature, increasing forward current ratings, and increase reliability of the device. Manufacturers of the IGBT would benefit by reducing time of production, materials, and cost by producing exposed junction IGBTs.

5.2 Future Work

First, future work suggestion begins with R134a refrigerant. The refrigerant was not intended for cooling power electronics; therefore the actual dielectric properties are not known. Voltage breakdown characteristics and a multi-year soak study would give a greater insight to the feasibility of cooling PEs.

Next, study of the effects of enhanced surfaces materials and flow impingement to assist in the heat transfer process. Enhanced surfaces such as metallic plates with small (< 0.001 in) ridges scored across the surface. The enhanced surface should assist with the

formation and departure of bubbles on the surface, which should increase the efficiency of the heat transfer of the submerged system. Flow impingement could increase the heat transfer by direct liquid jetting to the heat source. Flow impingement would ensure a fresh supply of liquid was in contact with the heat surface.

This thesis only considered steady state conditions, no thermal transients. Additional study of the thermal transients would help refine thermal model. Thermal transients are treated as impedances in the circuit diagram rather than pure resistance in the steady state model. While this is a good approximation, the thermal transients are in fact the temperature relation of one surface change due to a change in temperature from another surface. Thermal transients could give greater detail on the junction temperature as disturbances occur in the circuit.

Last, investigate further the exposed junction IGBT. Simulation has shown that exposing the junction to the cooling surface greatly reduces the junction temperature. Actual experimental data would verify the solution and provide additional insight into methods of heat removal using refrigerant.

List of References

[1] N. Mohan, T. M. Underland, W. P. Robbins, "Power Electronics, Converters, Applications, and Design," 3rd ed., John Wiley & Sons, Inc, 2003.

[2] *The Merriam-Webster Dictionary*, Springfield, Massachusetts, 1997.

[3] M. Lugwig, A. Gaedke, O. Slattery, J. Flannery, S. C. O'Mathuna, "Characterization of Cooling Curves for Power Device Die Attach using a Transient Cooling Curve Measurement," *IEEE Power Electronics Specialists Conference, 2000. PESC 00*, Vol. 3, 18-23 June 2000, pp. 1612 – 1617.

[4] I. Mudawar, "Direct-Immersion Cooling for High Power Electronic Chips," *InterSociety Conference on Thermal Phenomena in Electronics Systems*, 5-8 Feb. 1992, pp. 74-84.

[5] R-Theta, "FabFin Product Catalog," December 1, 1996.

[6] D. Faulkner, M. Khotan, R. Shekarriz, "Practical Design of a 1000W/cm^2 Cooling System," *Semiconductor Thermal Measurement and Management Symposium*, 11-13 March 2003, pp. 223-230.

[7] M. Saini, R. L. Webb, "Heat Rejection Limits of Air Cooled Plane Fin Heat Sinks for Computer Cooling," *IEEE Transactions on Computer and Packaging Technologies*, Vol. 26, No. 1, March 2003, pp. 71-79.

[8] K. Shenai, "Feasibility and Reliability of High-Temperature Power/Control Electronics for HEVs," A technical assessment prepared for Oak Ridge National Laboratories, 12 July 2004.

[9] J. S. Lai, K. Stanton, "Power Electronics Assessment – Vehicle System and Subsystem Interactions with Power Electronics," A technical assessment prepared for Oak Ridge National Laboratories, 30 June 2004.

[10] V. A. Sankaran, "Introducing the Power Electronics in Ford Hybrid Escape Vehicle," *IEEE Power Electronics Society Newsletter*, 3rd Quarter 2004, Vol. 16, No. 3, pp. 13-15.

[11] P. E. Phelan, V. A. Chiriac, T. T. Lee, "Current and Future Miniature Refrigeration Cooling Technologies for High Power Microelectronics," *IEEE Transactions on Component and Packaging Technologies*, Vol. 25, No. 3, September 2002, pp. 356-365.

[12] P. H. Desai, G. Wiegner, “Evaluation of Freon Modules for Power Electronics Design for a Locomotive Traction Drive,” *IEEE Transactions on Industry Applications*, Vol. 26, No. 3, May/June 1990, pp. 394-400.

[13] T. Jomard, U. Eckes, E. Touvier, ,M. Lallemand, “Modeling of the Two-Phase Cooling of a Power Semiconductor and its Associated Evaporators,” *Semiconductor Thermal Measurement and Management Symposium*, 1992. SEMI-THERM VIII., Eighth Annual IEEE , 3-5 Feb. 1992, pp.20 – 24

[14] C. Tantolin, M. Lallemand, U. Eckes, “Experimental Study of Immersion Cooling for Power Components,” *International Conference on Control*, 1994. Vol. 1., 21-24 Mar 1994, pp. 723-727.

[15] G. Major, General Motors, 28 September 2004, personal correspondence.

Appendices

Appendix I

International
IOR Rectifier

PD - 9.790

IRGBC20UD2

INSULATED GATE BIPOLAR TRANSISTOR
WITH ULTRAFAST SOFT RECOVERY DIODE

UltraFast CoPack IGBT

Features

- Switching-loss rating includes all "tail" losses
- HEXFRED™ soft ultrafast diodes
- Optimized for high operating frequency (over 5kHz)
  See Fig. 1 for Current vs. Frequency curve

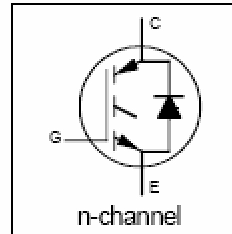

n-channel

$V_{CES} = 600V$

$V_{CE(sat)} \leq 3.0V$

$@V_{GE} = 15V, I_C = 6.5A$

Description

Co-packaged IGBTs are a natural extension of International Rectifier's well known IGBT line. They provide the convenience of an IGBT and an ultrafast recovery diode in one package, resulting in substantial benefits to a host of high-voltage, high-current, motor control, UPS and power supply applications.

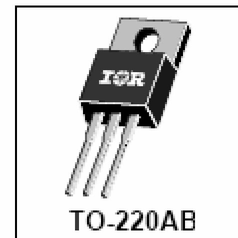

TO-220AB

Absolute Maximum Ratings

	Parameter	Max.	Units
V_{CES}	Collector-to-Emitter Voltage	600	V
I_C @ T_C = 25°C	Continuous Collector Current	13	A
I_C @ T_C = 100°C	Continuous Collector Current	6.5	
I_{CM}	Pulsed Collector Current ①	52	
I_{LM}	Clamped Inductive Load Current ②	52	
I_F @ T_C = 100°C	Diode Continuous Forward Current	7.0	
I_{FM}	Diode Maximum Forward Current	52	
V_{GE}	Gate-to-Emitter Voltage	± 20	V
P_D @ T_C = 25°C	Maximum Power Dissipation	60	W
P_D @ T_C = 100°C	Maximum Power Dissipation	24	
T_J T_{STG}	Operating Junction and Storage Temperature Range	-55 to +150	°C
	Soldering Temperature, for 10 sec.	300 (0.063 in. (1.6mm) from case)	
	Mounting Torque, 6-32 or M3 Screw.	10 lbf•in (1.1 N•m)	

Thermal Resistance

	Parameter	Min.	Typ.	Max.	Units
$R_{\theta JC}$	Junction-to-Case - IGBT	—	—	2.1	°C/W
$R_{\theta JC}$	Junction-to-Case - Diode	—	—	3.5	
$R_{\theta CS}$	Case-to-Sink, flat, greased surface	—	0.50	—	
$R_{\theta JA}$	Junction-to-Ambient, typical socket mount	—	—	80	
Wt	Weight	—	2 (0.07)	—	g (oz)

C-693

Revision 1

Electrical Characteristics @ T_J = 25°C (unless otherwise specified)

	Parameter	Min.	Typ.	Max.	Units	Conditions
$V_{(BR)CES}$	Collector-to-Emitter Breakdown Voltage ③	600	—	—	V	V_{GE} = 0V, I_C = 250µA
$\Delta V_{(BR)CES}/\Delta T_J$	Temp. Coeff. of Breakdown Voltage	—	0.69	—	V/°C	V_{GE} = 0V, I_C = 1.0mA
$V_{CE(on)}$	Collector-to-Emitter Saturation Voltage	—	2.2	3.0	V	I_C = 6.5A V_{GE} = 15V
		—	2.8	—		I_C = 13A See Fig. 2, 5
		—	2.5	—		I_C = 6.5A, T_J = 150°C
$V_{GE(th)}$	Gate Threshold Voltage	3.0	—	5.5		V_{CE} = V_{GE}, I_C = 250µA
$\Delta V_{GE(th)}/\Delta T_J$	Temp. Coeff. of Threshold Voltage	—	-11	—	mV/°C	V_{CE} = V_{GE}, I_C = 250µA
g_{fe}	Forward Transconductance ④	1.4	4.3	—	S	V_{CE} = 100V, I_C = 6.5A
I_{CES}	Zero Gate Voltage Collector Current	—	—	250	µA	V_{GE} = 0V, V_{CE} = 600V
		—	—	1700		V_{GE} = 0V, V_{CE} = 600V, T_J = 150°C
V_{FM}	Diode Forward Voltage Drop	—	1.4	1.7	V	I_C = 8.0A See Fig. 13
		—	1.3	1.6		I_C = 8.0A, T_J = 150°C
I_{GES}	Gate-to-Emitter Leakage Current	—	—	±100	nA	V_{GE} = ±20V

Switching Characteristics @ T_J = 25°C (unless otherwise specified)

	Parameter	Min.	Typ.	Max.	Units	Conditions	
Q_g	Total Gate Charge (turn-on)	—	16	22	nC	I_C = 6.5A	
Q_{ge}	Gate - Emitter Charge (turn-on)	—	2.5	3.8		V_{CC} = 400V	
Q_{gc}	Gate - Collector Charge (turn-on)	—	7.8	13		See Fig. 8	
$t_{d(on)}$	Turn-On Delay Time	—	60	—	ns	T_J = 25°C	
t_r	Rise Time	—	29	—		I_C = 6.5A, V_{CC} = 480V	
$t_{d(off)}$	Turn-Off Delay Time	—	130	200		V_{GE} = 15V, R_G = 50Ω	
t_f	Fall Time	—	65	120		Energy losses include "tail" and	
E_{on}	Turn-On Switching Loss	—	0.21	—	mJ	diode reverse recovery.	
E_{off}	Turn-Off Switching Loss	—	0.22	—		See Fig. 9, 10, 11, 18	
E_{ts}	Total Switching Loss	—	0.43	0.65			
$t_{d(on)}$	Turn-On Delay Time	—	60	—	ns	T_J = 150°C, See Fig. 9, 10, 11, 18	
t_r	Rise Time	—	30	—		I_C = 6.5A, V_{CC} = 480V	
$t_{d(off)}$	Turn-Off Delay Time	—	210	—		V_{GE} = 15V, R_G = 50Ω	
t_f	Fall Time	—	180	—		Energy losses include "tail" and	
E_{ts}	Total Switching Loss	—	0.71	—	mJ	diode reverse recovery.	
L_E	Internal Emitter Inductance	—	7.5	—	nH	Measured 5mm from package	
C_{ies}	Input Capacitance	—	330	—	pF	V_{GE} = 0V	
C_{oes}	Output Capacitance	—	65	—		V_{CC} = 30V See Fig. 7	
C_{res}	Reverse Transfer Capacitance	—	6.0	—		f = 1.0MHz	
t_{rr}	Diode Reverse Recovery Time	—	37	55	ns	T_J = 25°C See Fig.	
		—	55	90		T_J = 125°C 14	I_F = 8.0A
I_{rr}	Diode Peak Reverse Recovery Current	—	3.5	5.0	A	T_J = 25°C See Fig.	
		—	4.5	8.0		T_J = 125°C 15	V_R = 200V
Q_{rr}	Diode Reverse Recovery Charge	—	65	138	nC	T_J = 25°C See Fig.	
		—	124	360		T_J = 125°C 16	di/dt = 200A/µs
$di_{(rec)M}/dt$	Diode Peak Rate of Fall of Recovery	—	240	—	A/µs	T_J = 25°C See Fig.	
	During t_b	—	210	—		T_J = 125°C 17	

Notes:

① Repetitive rating; V_{GE}=20V, pulse width limited by max. junction temperature. (See fig. 20)

② V_{CC}=80%(V_{CES}), V_{GE}=20V, L=10µH, R_G= 50Ω, (See fig. 19)

③ Pulse width ≤ 80µs; duty factor ≤ 0.1%.

④ Pulse width 5.0µs, single shot.

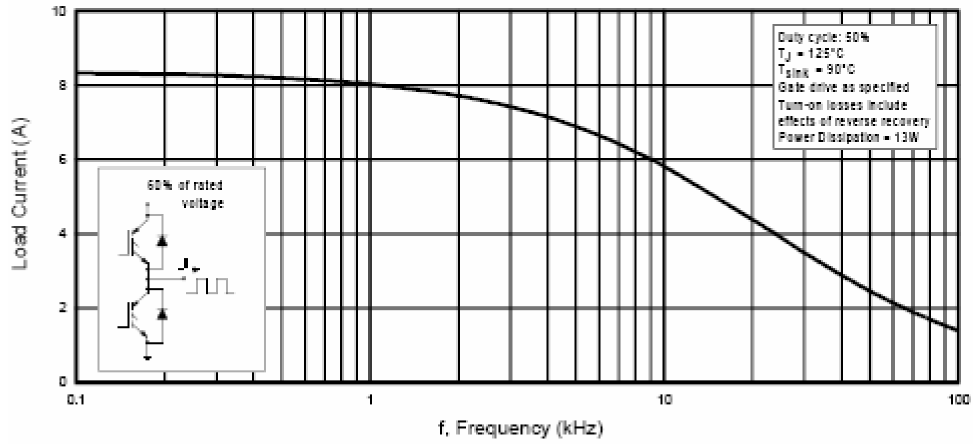

Fig. 1 - Typical Load Current vs. Frequency
(Load Current = I_{RMS} of fundamental)

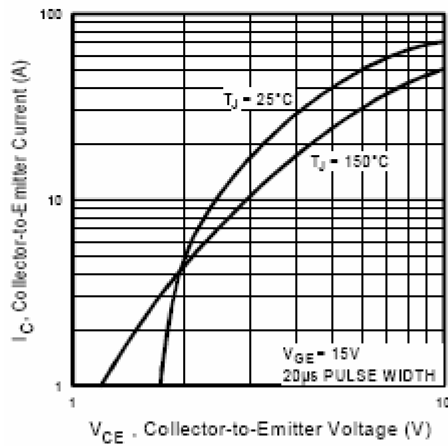

Fig. 2 - Typical Output Characteristics

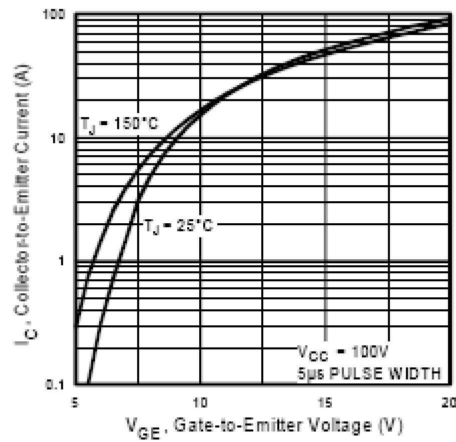

Fig. 3 - Typical Transfer Characteristics

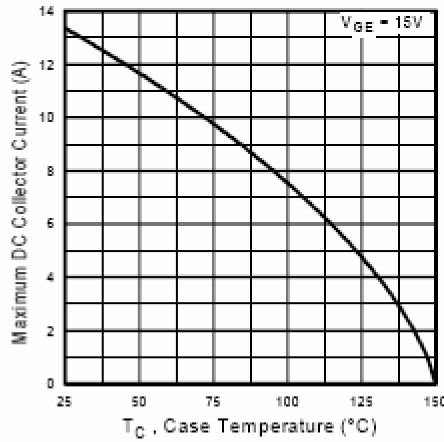

Fig. 4 - Maximum Collector Current vs. Case Temperature

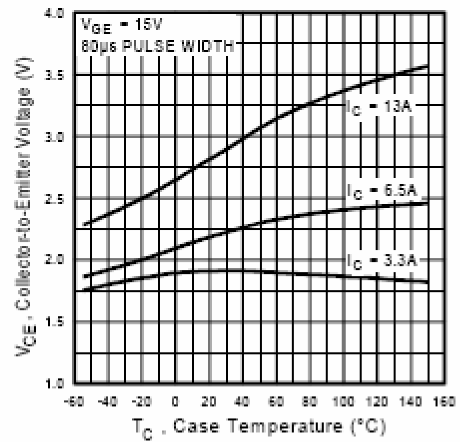

Fig. 5 - Collector-to-Emitter Voltage vs. Case Temperature

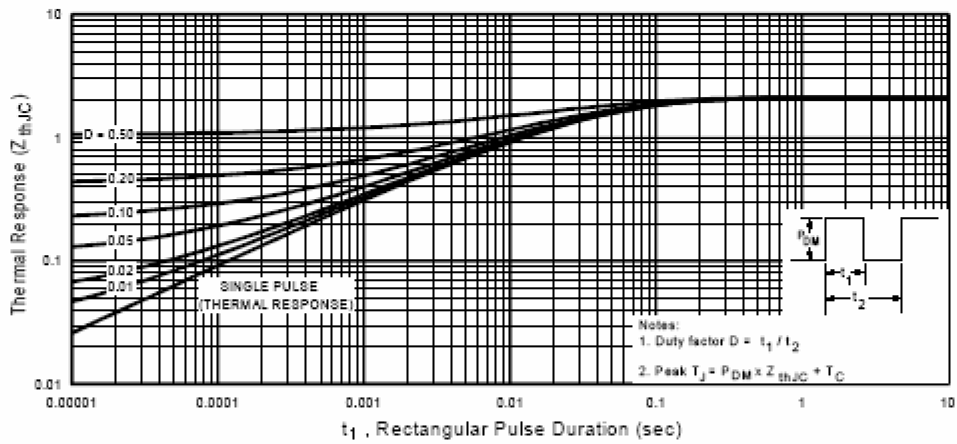

Fig. 6 - Maximum IGBT Effective Transient Thermal Impedance, Junction-to-Case

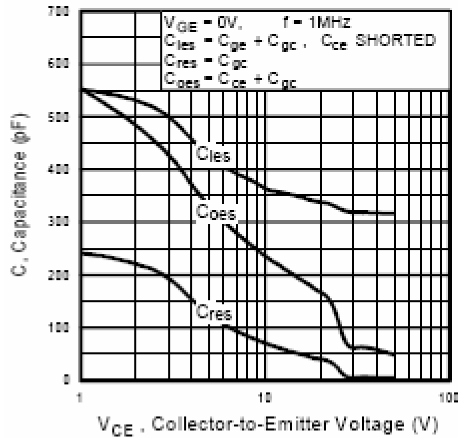

Fig. 7 - Typical Capacitance vs. Collector-to-Emitter Voltage

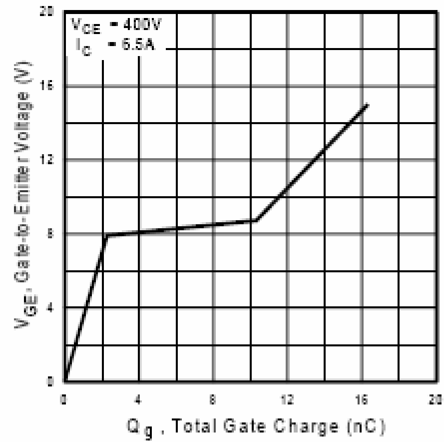

Fig. 8 - Typical Gate Charge vs. Gate-to-Emitter Voltage

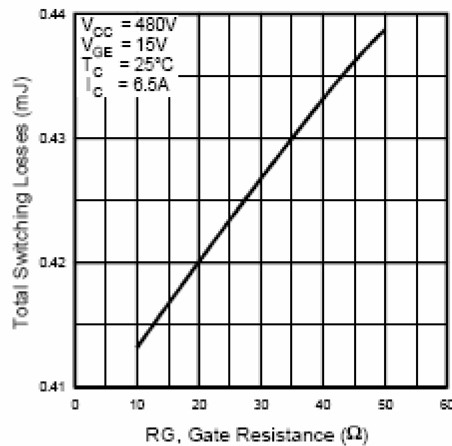

Fig. 9 - Typical Switching Losses vs. Gate Resistance

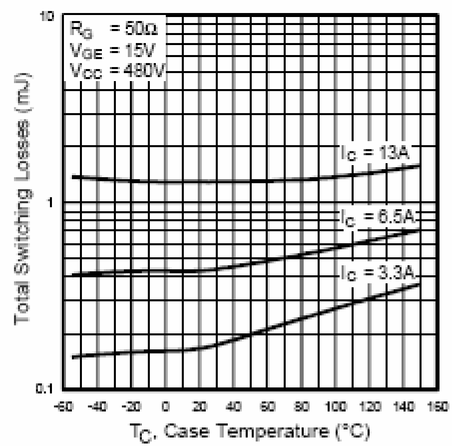

Fig. 10 - Typical Switching Losses vs. Case Temperature

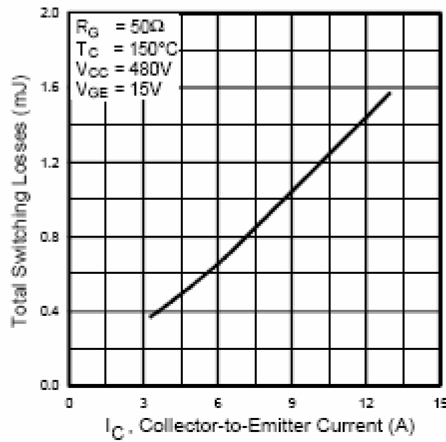

Fig. 11 - Typical Switching Losses vs. Collector-to-Emitter Current

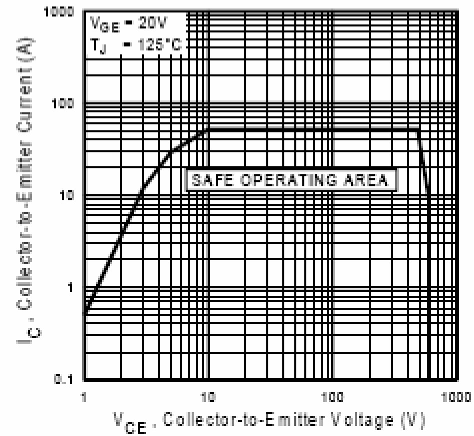

Fig. 12 - Turn-Off SOA

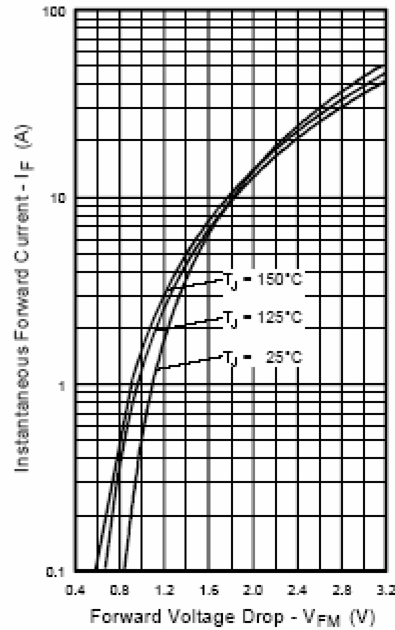

Fig. 13 - Maximum Forward Voltage Drop vs. Instantaneous Forward Current

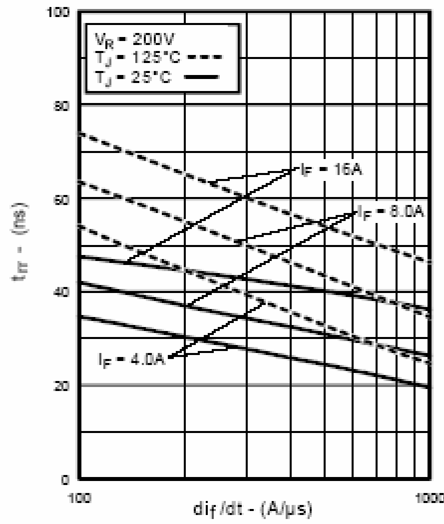

Fig. 14 - Typical Reverse Recovery vs. di_f/dt

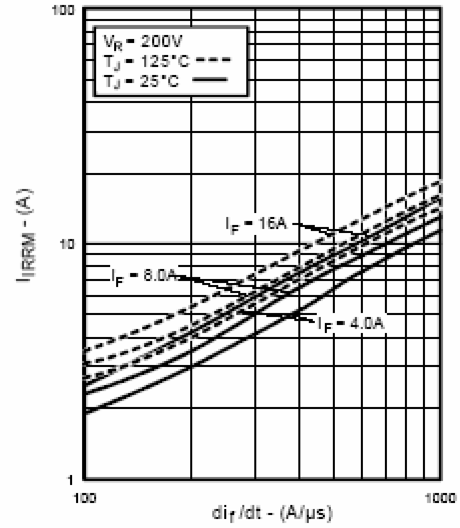

Fig. 15 - Typical Recovery Current vs. di_f/dt

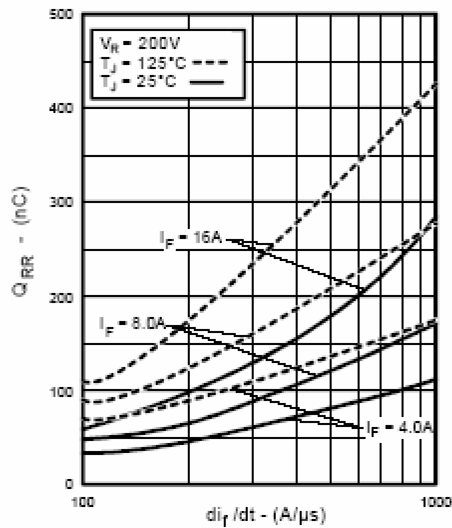

Fig. 16 - Typical Stored Charge vs. di_f/dt

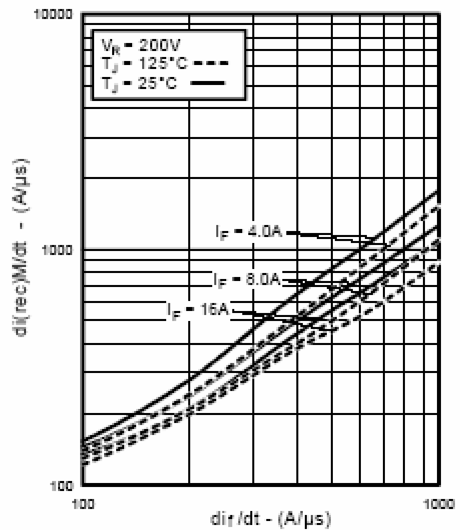

Fig. 17 - Typical $di_{(rec)M}/dt$ vs. di_f/dt

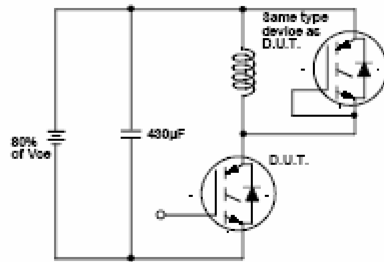

Fig. 18a - Test Circuit for Measurement of I_{LM}, E_{on}, $E_{off(diode)}$, t_{rr}, Q_{rr}, I_{rr}, $t_{d(on)}$, t_r, $t_{d(off)}$, t_f

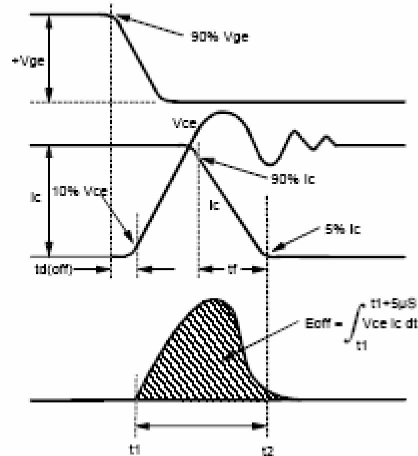

Fig. 18b - Test Waveforms for Circuit of Fig. 18a, Defining E_{off}, $t_{d(off)}$, t_f

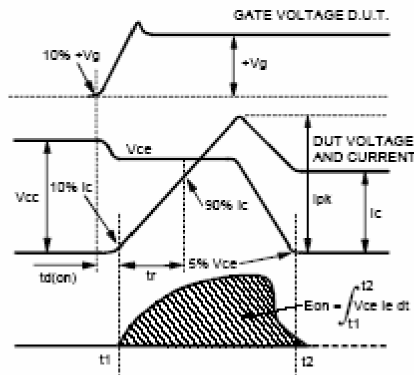

Fig. 18c - Test Waveforms for Circuit of Fig. 18a, Defining E_{on}, $t_{d(on)}$, t_r

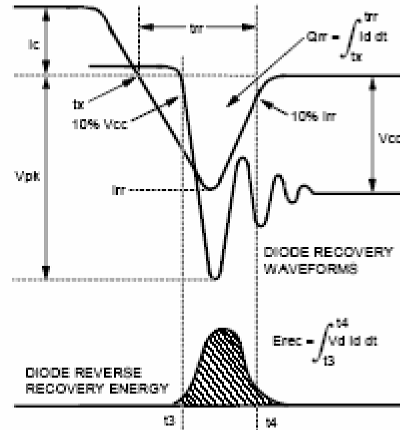

Fig. 18d - Test Waveforms for Circuit of Fig. 18a, Defining E_{rec}, t_{rr}, Q_{rr}, I_{rr}

Refer to Section D for the following:
Appendix D: Section D - page D-6
Fig. 18e - Macro Waveforms for Test Circuit Fig. 18a
Fig. 19 - Clamped Inductive Load Test Circuit
Fig. 20 - Pulsed Collector Current Test Circuit

Package Outline 1 - JEDEC Outline TO-220AB **Section D - page D-12**

Appendix II

List of Equipment

1. International Rectifier, Insulated Gate Bipolar Transistor, Model No. IRGBC20UD2

2. Dell Latitude D600 notebook computer

3. National Instruments DAQCard 1200, 8 inputs, 2 outputs, 100 kS/s, 12 bit Multifunction I/O

4. Yokogawa PZ4000 Power Analyzer, DC 2 MHz, 5 MS/s

5. Xantrex DC Power Supply XPR 600-10, 600 V, 10 A

6. Agilent 33250A Function Generator

7. Power Designs, Inc. DC Power Supply, 20.0 V, 1.0 A

8. Dale NH-250 Power Resistor, 250 W, 40 Ω and 80 Ω

9. Vishay Electro-Films, Inc. 10 Ω, Thin-Film Resistors

10. Thermistor Model No. 44008

11. R134a Refrigerant, Dupont

12. 2003 Buick Park Avenue Air Conditioning System comprised of the compressor, evaporator, condenser, and control system

Appendix III

Early in the experimentation phase, a need for an automated means to record temperatures quickly arose. Thermistors, notebook computer, national instruments data acquisition card, and LabView software were the equipment available. A LabView program was written to sample the 8 eight theristor temperatures, store the samples in a spreadsheet format, display the instantaneous temperatures, and plot a histogram of the temperatures. The user panel is shown in Figure A.1.

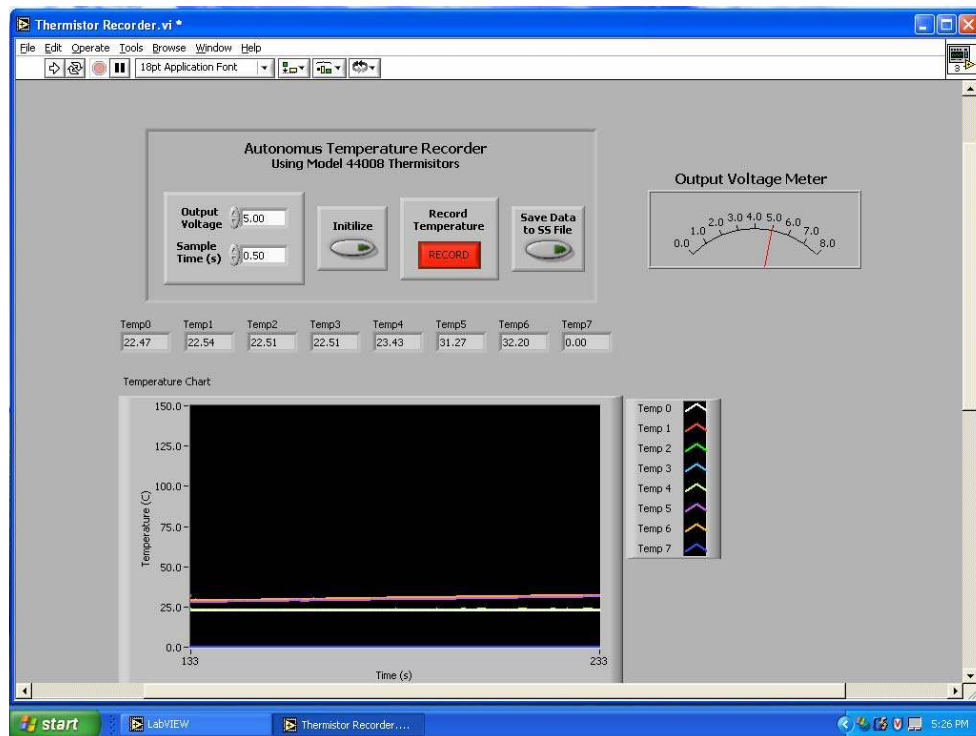

Figure A.1. Temperature recorder program user interface

Vita

Jeremy B. Campbell has been actively involved in the study of electricity since 1992 beginning with Industrial Electricity at Fayette Plateau Vocational Center. From there, he continued his studies of electricity at West Virginia Institute of Technology from September 1994 to December 1999 graduating with a Bachelors Degree in Electrical Engineering, while earning a Journeyman's Electricians Licenses in 1995. He began his professional career in 2000 for the Department of Defense as a civilian performing various electrical studies including power systems analysis. During his graduate studies, Jeremy joined the Post-Graduate Program with the Power Electronics and Electric Machines Research Center at Oak Ridge National Laboratory, where he performed research in HEVs including the research contained in this thesis. He plans to continue his career in the power electronics and power systems industry.